

TACO: Taming Diffusion for in-the-wild Video Amodal Completion

Ruijie Lu^{1,2*}, Yixin Chen^{2†}, Yu Liu^{2,3}, Jiayang Tang¹,
Junfeng Ni^{2,3}, Diwen Wan¹, Gang Zeng^{1†}, Siyuan Huang^{2†}

* Work done as an intern at BIGAI † Corresponding Author

¹ State Key Laboratory of General Artificial Intelligence, Peking University

² State Key Laboratory of General Artificial Intelligence, BIGAI ³ Tsinghua University

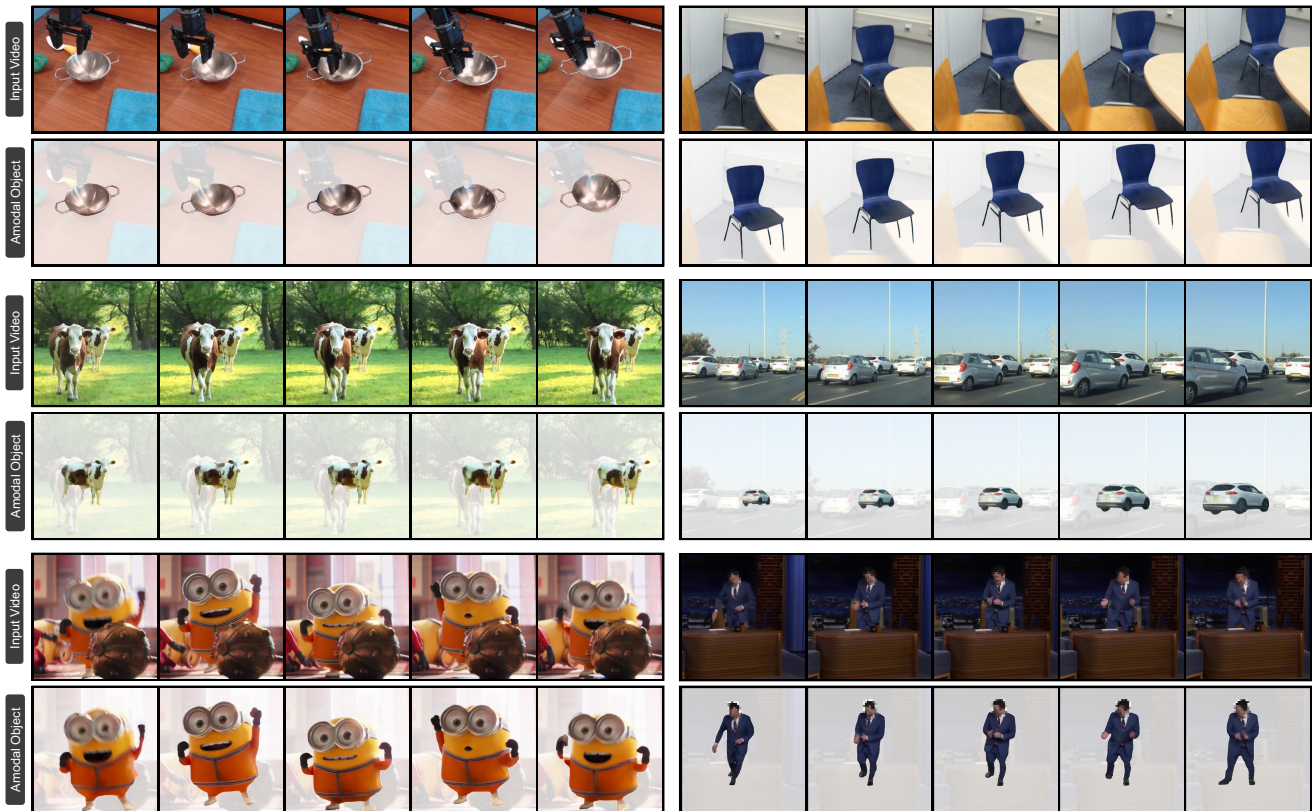


Figure 1. We propose **TACO** for video amodal completion. Our model is capable of synthesizing consistent amodal contents in diverse in-the-wild occluded scenarios, including robotic manipulation, scene understanding, autonomous driving, and Internet videos.

Abstract

Humans can infer complete shapes and appearances of objects from limited visual cues, relying on extensive prior knowledge of the physical world. However, completing partially observable objects while ensuring consistency across video frames remains challenging for existing models, especially for unstructured, in-the-wild videos. This paper tackles the task of Video Amodal Completion (VAC), which aims to generate the complete object consistently throughout the video given a visual prompt specifying the object of

interest. Leveraging the rich, consistent manifolds learned by pre-trained video diffusion models, we propose a conditional diffusion model, **TACO**, that repurposes these manifolds for VAC. To enable its effective and robust generalization to challenging in-the-wild scenarios, we curate a large-scale synthetic dataset with multiple difficulty levels by systematically imposing occlusions onto un-occluded videos. Building on this, we devise a progressive fine-tuning paradigm that starts with simpler recovery tasks and gradually advances to more complex ones. We demonstrate **TACO**'s versatility on a wide range of in-the-wild videos

from Internet, as well as on diverse, unseen datasets commonly used in autonomous driving, robotic manipulation, and scene understanding. Moreover, we show that **TACO** can be effectively applied to various downstream tasks like object reconstruction and pose estimation, highlighting its potential to facilitate physical world understanding and reasoning. Our project page is available at <https://jason-aplp.github.io/TACO/>.

1. Introduction

Humans excel at inferring complete shapes and appearances of partially observable objects, as explained by the continuity and closure principle from Gestalt psychology [46, 87, 93, 94]. This capability is challenging for current models when it requires consistently completing a target object across frames and generalizing to diverse in-the-wild videos, due to the innate ambiguities in unobserved areas. Such consistent amodal representations are crucial for physical world understanding, supporting reasoning [60] and facilitating downstream tasks like reconstruction [10, 58, 65, 66, 89–91, 110], robotics [6, 50, 59, 61, 82, 117], autonomous driving [11, 64], and beyond. Therefore, it is vital to develop a model’s “consistent see through” capability, especially when applied to diverse in-the-wild videos.

In this paper, we tackle the task of Video Amodal Completion (VAC), recovering spatio-temporal consistent and complete objects given occluded observations in a video. Previous work mainly focuses on related but distinct aspects of visual content completion. Image amodal completion [67, 100, 112] and inpainting [37, 63, 81] can be extended to videos by processing each frame independently, but they ignore neighboring frames and fail to predict amodal objects consistently. Video inpainting [24, 42, 43, 47, 52, 111] can also be adapted to this problem. However, these methods require specifying masks, implying the complete shape of occluded objects. Additionally, they do not possess strong object awareness, resulting in obvious artifacts when completing occluded objects in videos [50].

Building on advances in video generation [4, 28, 32, 99], we repurpose pre-trained models, which have learned rich spatio-temporally consistent manifolds from Internet-scale datasets [3], for amodal completion. We introduce **TACO**, a conditional video diffusion model, that given a video and a visual prompt specifying an object, generates its consistent amodal representation across frames.

Our key insight lies in how to effectively fine-tune the model for better generalization and robustness across diverse, challenging scenarios. Simulator data [35] inherently suffers from a sim-to-real gap, while real-world videos lack ground-truth amodal references for occluded objects. Inspired by pix2gestalt [67], we utilize real-world videos and curate a diverse, scalable synthetic dataset by identifying unoccluded objects in videos and then overlaying occluders

consistently. As shown in SAM2 [72], training on increasingly more challenging data is beneficial for generalization. Thus, we adopt a *model-in-the-loop* approach that identifies failures and difficult data samples to guide subsequent data augmentation. This results in roughly 200k video pairs at varying difficulty levels. We then employ a progressive training strategy, beginning with simpler recovery tasks and gradually advancing to more complex ones, which is critical for robust generalization to challenging in-the-wild videos.

Extensive experiments demonstrate that our method can synthesize consistent amodal objects in shape, appearance, and motion. It generalizes well to unseen datasets like BridgeData [19, 88], ScanNet [14, 106] and in-the-wild Internet videos, as shown in Fig. 1. Our model also achieves state-of-the-art performance on Video Amodal Segmentation (VAS) in a zero-shot manner. Beyond the model’s “see-through” capability, we show our model can directly facilitate downstream tasks as a drop-in module in object reconstruction and 6-DoF pose estimation.

To sum up, our main contributions are:

1. We propose **TACO**, a conditional video diffusion model for Video Amodal Completion (VAC), enabling spatio-temporally consistent recovery of amodal objects from monocular video in occluded scenarios.
2. We present a scalable data curation pipeline for constructing occluded and unoccluded video pairs as well as a progressive training paradigm for effective and robust generalization to unseen in-the-wild scenarios.
3. Experiments show that our approach outperforms all previous methods in Video Amodal Completion and performs on par with SOTA in Video Amodal Segmentation in a zero-shot manner. Furthermore, we directly leverage our model to improve downstream tasks like object reconstruction and 6-DoF pose estimation, highlighting its potential in real-world applications.

2. Related Work

Amodal Segmentation and Completion Amodal completion is challenging due to the ambiguity in occluded regions. Most previous works focus on simpler tasks, such as amodal segmentation [41, 54, 68, 73, 116] or detection [38], predicting amodal segmentation masks or bounding boxes. Follow-up studies [2, 15, 21, 33, 35, 84, 105] extend amodal segmentation to the video domain to ensure consistency. However, these approaches do not generate content for occluded areas. More recent works [67, 100, 112] attempt to unleash the capabilities of pre-trained diffusion models [75] to generate content for these areas. Nevertheless, these models are limited to the image level, making it difficult to maintain spatial-temporal consistency and utilize information from neighboring frames, which often reveal occluded parts from alternative viewpoints and provide valuable context for generating coherent content. Instead, we propose to

address this task directly within the video domain, enabling a broader receptive field across the entire video and synthesizing more consistent results. Concurrent work [9] also explores video amodal completion in two stages by first predicting amodal masks; however, its reliance on simulation data, *i.e.*, SAIL-VOS [35], and the prerequisite of pseudo-depth limit its applicability in more generalized use cases.

Video Inpainting Video inpainting, which fills masked areas with plausible and consistent content, can also be repurposed for Video Amodal Completion (VAC). Early explorations mainly focus on how to transfer information from neighboring frames to the target frame [69] using 3D convolutions [8, 36], flow [24, 52, 102], or cross-attention [47, 48, 56]. More recently, research work [95, 115] proposes to incorporate text prompts when inpainting a video, leveraging powerful text-based image inpainting techniques [13, 63]. However, all these inpainting-based methods require specifying masked regions, which is non-trivial since we do not know the occluded object’s shape. Furthermore, video inpainting models are proposed for more general visual completion; they lack amodal object awareness, making it difficult to accurately recover occluded portions of objects, even when provided with a precise inpainting mask [50].

Video Diffusion Models We have witnessed huge advances in video generation [1, 4, 5, 25, 28, 30, 32, 78, 99, 104] recently, with most approaches being diffusion-based, building on the success of text-to-image diffusion models [71, 75, 76]. Leveraging the rich and consistent manifolds learned by large-scale video diffusion models, subsequent works have explored repurposing these pre-trained models for novel tasks such as depth estimation [27, 34, 40, 77, 103], novel view synthesis (NVS) [55, 57, 62, 85, 108], assets generation [86, 98, 118], and so on [51, 53]. In this work, we tackle the challenging task of video amodal completion. We use publicly available Stable Video Diffusion (SVD) [4], introducing a scalable dataset and employing a progressive training paradigm for effective fine-tuning.

3. Data Curation

For the training and evaluation of the VAC task, we curate a large-scale dataset, Object-video-Overlay (OvO). Ideally, a VAC dataset should comprise diverse real-world videos containing occluded objects alongside their unoccluded versions. While such data pairs can be scalably generated in simulated environments [12, 96], relying solely on simulator data inevitably introduces a sim-to-real gap [31], limiting generalization capability. Contrarily, collecting such data pairs at scale in the real world is costly and impractical, as it requires removing occluders while replicating the motion of both the camera and other dynamics within a scene.

Inspired by previous works on image amodal segmentation [23, 49, 67], we construct our dataset automatically

by identifying amodal objects in videos and overlaying occlusions. Yet, naively placing occluders randomly in each frame introduces flickering, compromising consistency. As explained in SAM2 [72], progressive training on increasingly challenging data enhances model performance. However, it remains unclear what modes of data are more challenging, necessitating a model-in-the-loop approach, where model feedback guides data augmentation. As a result, we finally curate the OvO dataset with two difficulty levels: OvO-Easy and OvO-Hard. The overall curation pipeline, illustrated in Fig. 2, consists of three steps.

Identify Candidate We start by collecting real-world videos from diverse sources, including MVIImgNet [109], Bdd100k [107], and SA-V [72]. Object instances are segmented within videos using either provided annotations [72, 107] or off-the-shelf segmentation models [74].

Amodal Check We then identify high-quality and fully visible candidates using provided annotations [107] or a combination of heuristic rules and manual filtering. The heuristic rules are based on three main criteria: (1) Instances surrounded by regions closer to the camera, are likely to be occluded; (2) Tiny segmentations or those touching boundaries imply less prominent objects; and (3) Segmentations with numerous internal holes are likely of low quality.

Progressive Occlusion Overlay Once suitable amodal candidates are selected, we apply occlusions by consistently overlaying images of occluders sourced from SA-1B [45].

We begin by constructing a OvO-Easy dataset with a relatively naive yet consistent occlusion overlay strategy. Occlusions are guaranteed in both the first and last frame, with an occlusion rate between 0.3 and 0.7. To create smooth and consistent motion throughout the video, the occluders’ positions are linearly interpolated across intermediate frames.

During iterative testing, we identify failure cases where the model struggles, such as regions with severe or persistent occlusions, uncommon or swift object motions, and occlusions caused by close or direct contact. Guided by these observations, we further curate an OvO-Hard dataset with a more aggressive occlusion overlay strategy, featuring a more challenging setting. It first sets the occluder’s position in the first frame, maintaining an occlusion rate between 0.4 and 0.8. The occluder then moves in tandem with the amodal candidate’s bounding box, dynamically adjusting its size according to changes in the candidate’s bounding box. This not only results in a higher occlusion rate compared to OvO-Easy but also introduces a “persistent occlusion” effect, where a portion of the candidate is likely to be persistently occluded throughout the video, necessitating a stronger completion capability. To further enhance realism, image feathering techniques are applied, softening occlusion boundaries for mimicking occlusions by close contact.

In addition to progressive occlusion overlays, the choice of data sources plays a crucial role. To boost the diversity

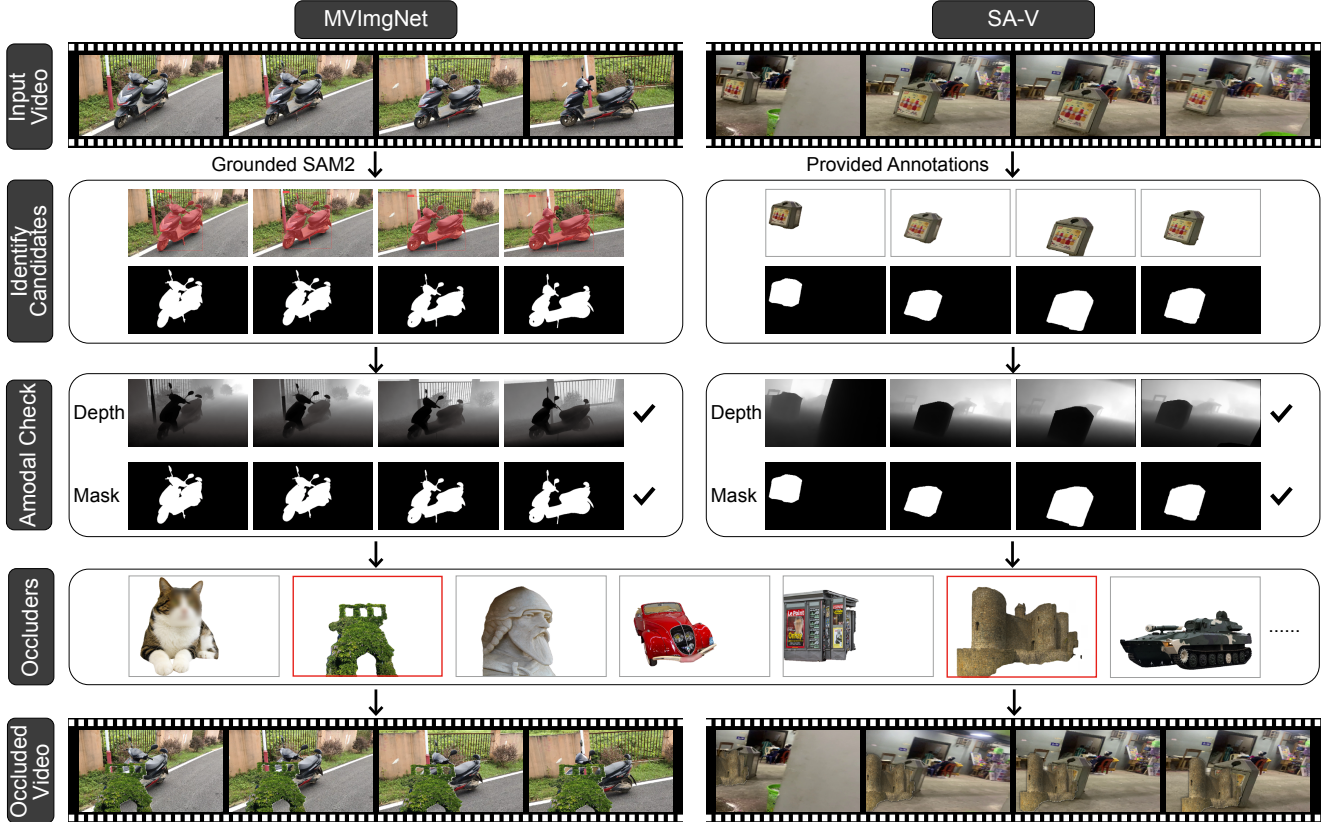


Figure 2. **Data curation pipeline.** We generate our synthetic custom dataset following three steps. First, given an input video, we identify possibly unoccluded candidates using an off-the-shelf segmentation model [74] or provided annotations. Next, we check whether the candidate is amodal with heuristic rules and manual filtering. Finally, we select an occluder and overlay it upon the candidate consistently.

of OvO-Hard, we incorporate image-level datasets, which offer a broader range of object instances with precise annotations. Specifically, we select complete object instances from SA-1B [45] and apply various image transformation techniques, such as zooming, parallel moving, and warping, to simulate camera movement and object dynamics. These transformed images are then sequenced into synthetic videos, to which we apply the same curation strategy used for video data. An illustration of these image transformation techniques is provided in *supplementary materials*.

4. Method

We address the task of Video Amodal Completion (VAC). Formally, given a video $\mathbf{v} \in \mathbb{R}^{T \times H \times W \times 3}$ and prompt p , which is a point or mask identifying the object of interest, the target model f aims to recover a consistent unoccluded video of the object $\mathbf{o} \in \mathbb{R}^{T \times H \times W \times 3}$, *i.e.*,

$$\mathbf{o} = f(\mathbf{v}, p). \quad (1)$$

Given a prompt p , we use SAM2 [72] to obtain visible masks of the object in a video. Key insights of our model lie in leveraging the pre-trained video diffusion models and

progressively fine-tuning them on our scalable dataset to ensure robust generalization to in-the-wild scenarios. An illustrative overview is provided in Fig. 3.

4.1. Preliminaries of Video Diffusion Models

Diffusion models [29, 79] learn a target data distribution $p(\mathbf{x})$ by gradually adding noise and then iteratively denoising. In the context of video diffusion, a sample $\mathbf{x}_0 \sim p(\mathbf{x})$ represents a video, and we choose the publicly available Stable Video Diffusion (SVD) [4] as our base model in this paper. SVD adopts an EDM-framework [39] as the noise scheduler. In the forward process, i.i.d. Gaussian noise with σ_t^2 -variance will be added to the data $\mathbf{x}_0 \sim p(\mathbf{x})$:

$$\mathbf{x}_t = \mathbf{x}_0 + \sigma_t^2 \epsilon, \quad \epsilon \sim \mathcal{N}(\mathbf{0}, \mathbf{I}). \quad (2)$$

$\mathbf{x}_t \sim p(\mathbf{x}; \sigma_t)$ stands for the data with noise level σ_t , and when the noise level is large enough, denoted as σ_{\max} , the distribution will be indistinguishable from pure Gaussian noise. Building on this fact, SVD starts from a high-variance Gaussian noise $\mathbf{x}_M \sim \mathcal{N}(\mathbf{0}, \sigma_{\max}^2 \mathbf{I})$, and gradually denoise it towards $\sigma_0 = 0$ for clean data using a learnable

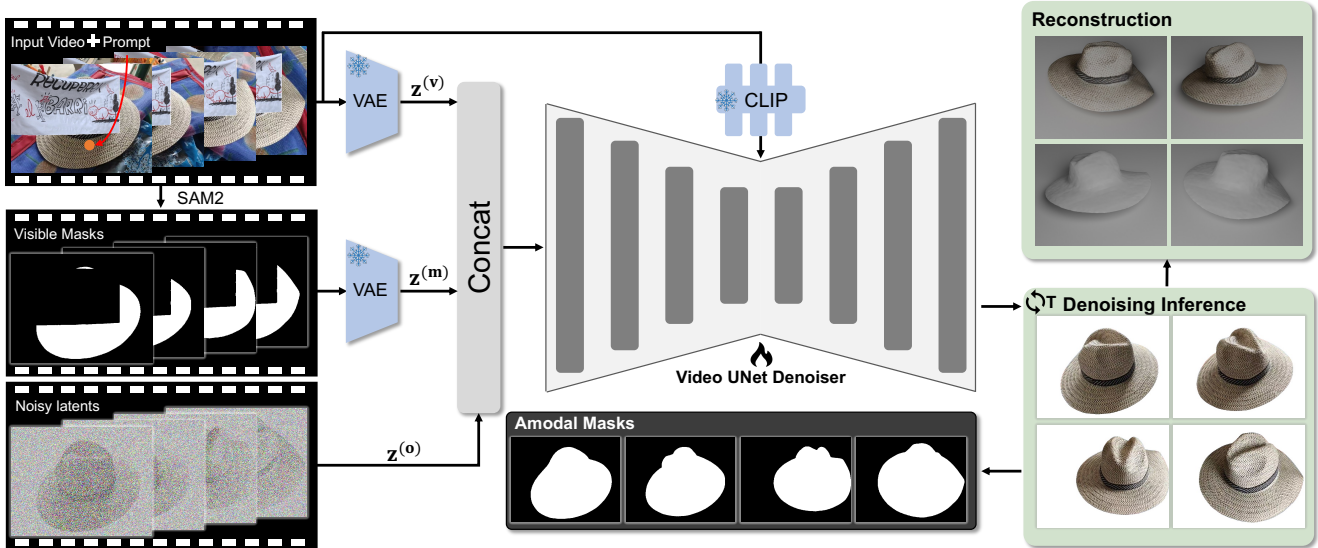


Figure 3. **Method overview.** We propose **TACO**, a conditional video diffusion model for Video Amodal Completion (VAC). **TACO** takes an occluded video and a visual prompt (point or mask) as input and synthesizes a consistent and complete object throughout the video.

denoiser D_θ , which is trained via denoising score matching:

$$\mathbb{E}_{\mathbf{x}_t \sim p(\mathbf{x}; \sigma_t), \sigma_t \sim p(\sigma)} [\lambda_{\sigma_t} \|D_\theta(\mathbf{x}_t; \sigma_t; \mathbf{c}) - \mathbf{x}_0\|_2^2], \quad (3)$$

where $p(\sigma)$ is the noise level distribution, \mathbf{c} is the conditional information, and λ_{σ_t} is the loss weight at time t .

4.2. TACO

As shown in Fig. 3, our proposed method builds upon a pre-trained video diffusion model, aiming to consistently complete a target object given an occluded video \mathbf{v} and the object’s corresponding visible masks.

Conditioning on an entire video Video diffusion models typically use two types of conditional guidance: (1) High-level conditioning that leverages CLIP [70] embedding of a reference image y via cross-attention in the U-Net, and (2) Low-level conditioning that concatenates VAE [44] encoded reference images with noisy frames $\mathbf{x}_t^{1:N}$ along the channel dimension as input to the U-Net.

SVD [4] conditions on a single reference image. In our VAC task, however, the entire video serves as input, requiring a conditioning mechanism that spans all frames. Inspired by previous works [34, 77, 85] and as illustrated in Fig. 3, we directly concatenate the input video latent $\mathbf{z}^{(v)}$ with the noisy object video latent $\mathbf{z}^{(o)}$. To incorporate high-level semantic information, we inject frame-wise CLIP embeddings into corresponding frames of the denoising U-Net through cross-attention. This design provides the model with a broad receptive field, enabling it to access information from all frames simultaneously, which is crucial for maintaining consistency when decoding amodal objects.

The visible masks $\mathbf{m} \in \mathbb{R}^{T \times H \times W}$, pinpointing the object of interest and mitigating the risk of hallucinating irrel-

evant content, are encoded into the same latent space as the input video, denoted as $\mathbf{z}^{(m)}$. These latent masks are concatenated with the video latents $\mathbf{z}^{(v)}$ and the noisy object latents $\mathbf{z}^{(o)}$, forming the final input to the denoising U-Net.

Progressive training strategy Inspired by SAM2 [45] which improves performance by learning from increasingly harder data, we adopt a similar progressive training strategy. In *Phase 1*, we start training from a relatively simple dataset, OvO-Easy, possessing a low occlusion rate and few “persistent occlusion” as explained in Sec. 3. This dataset draws exclusively from MVImgNet [109] and SA-V [72], facilitating a smooth initial training phase. Through iterative testing, we identify failure cases where the model struggles, such as regions with severe or persistent occlusions, uncommon or swift object motions, and occlusions caused by close or direct contact. In response, we further curate the OvO-Hard dataset and continue *Phase 2* training. This involves adopting a more aggressive occlusion overlay strategy, incorporating more diverse sources from image-level dataset SA-1B [45], and applying image feathering techniques to create more realistic occlusions. To further validate the effectiveness of progressive fine-tuning, we continue training the *Phase 1* and *Phase 2* checkpoints on an autonomous driving dataset Bdd100k [107], which is curated using the same strategy to curate OvO-Hard but possesses a dramatically different resolution compared to OvO-Easy and OvO-Hard. The ablative results of progressive training are presented in Sec. 5.2. As mentioned by previous works [51, 85], SVD struggles with substantial resolution changes, so we refrain from joint training on this split.

Tackling long videos Current video generative models [4, 32, 99], including ours, are constrained by a fixed frame

Table 1. **Quantitative comparison on amodal completion and segmentation.** We evaluate on four synthetic datasets, and our method outperforms baselines in terms of image alignment, mask alignment, and cross-frame consistency.

Dataset	Method	Image Alignment			Mask Alignment	Frame Consistency	
		PSNR(\uparrow)	SSIM(\uparrow)	LPIPS(\downarrow)	IoU(\uparrow)	CLIP-T(\uparrow)	FVD(\downarrow)
OvO-Easy	Pix2Video	12.590	0.682	0.368	42.1	0.937	1561.10
	E ² FGVI	13.385	0.664	0.306	59.8	0.964	1015.17
	pix2gestalt	20.699	0.829	0.109	88.9	0.926	389.77
	Ours	26.110	0.906	0.054	95.6	0.976	142.37
OvO-Hard	Pix2Video	11.873	0.662	0.402	35.2	0.945	1715.87
	E ² FGVI	12.861	0.639	0.346	59.5	0.967	1260.60
	pix2gestalt	18.184	0.777	0.157	83.7	0.913	674.24
	Ours	22.573	0.857	0.093	92.4	0.979	291.49
Kubric-Static	Pix2Video	14.181	0.680	0.338	34.1	0.936	1166.68
	E ² FGVI	14.194	0.684	0.230	57.5	0.964	738.05
	pix2gestalt	20.516	0.822	0.125	75.6	0.915	382.67
	PCNet	19.848	0.857	0.118	83.2	0.959	254.08
	Ours	23.963	0.891	0.073	83.9	0.970	162.91
Kubric-Dynamic	Pix2Video	15.571	0.728	0.311	20.8	0.942	979.57
	E ² FGVI	14.617	0.691	0.224	50.6	0.969	726.55
	pix2gestalt	19.676	0.830	0.132	68.3	0.906	429.11
	PCNet	20.373	0.864	0.104	76.2	0.957	253.45
	Ours	23.054	0.886	0.080	77.4	0.970	209.28

number. To overcome this, we introduce a sliding window mechanism that incrementally synthesizes future frames based on previously generated outputs. To be specific, given a video clip $\mathbf{v}^{1:N}$, where N is the total frame number, our model begins with the initial $\mathbf{v}^{1:k}$ ($k = 14$) frames, producing a completed object video $\mathbf{o}^{1:k}$. The synthesized object is then reintegrated into the video as:

$$\tilde{\mathbf{v}}^{1:k} = \mathbf{o}^{1:k} \odot \mathcal{M} + \mathbf{v}^{1:k} \odot (1 - \mathcal{M}), \quad (4)$$

where \mathcal{M} denotes the object mask area obtained from $\mathbf{o}^{1:k}$ and \odot represents pixel-wise product. In the next iteration of completion, our model takes as input the concatenation of previously generated frames and the next sequence of frames, denoted as $[\tilde{\mathbf{v}}^{(k-m+1):k}; \mathbf{v}^{(k+1):(2k-m)}]$, where $m = 5$ represents the sliding window size. This process iterates until the entire video clip is processed. By reinserting the synthesized objects into subsequent frames, the model preserves better consistency across long video sequences.

5. Experiment

5.1. Video Amodal Completion and Segmentation

Setup Video Amodal Segmentation (VAS) predict the amodal masks of occluded objects consistently across video frames, while Video Amodal Completion (VAC) requires further filling in reasonable content. We quantitatively benchmark VAC on four datasets: OvO-Easy, OvO-Hard, Kubric-Static, Kubric-Dynamic [18, 26], and VAS on two datasets: MOVi-B and MOVi-D [21]. We also conduct a

user study on 20 in-the-wild [14, 19, 88, 101, 106, 107] and Internet videos. Details are in *supplementary materials*.

Baselines and Metrics We compare our method against image-level amodal completion approaches, pix2gestalt [67] and PCNet [113], a video inpainting method E²FGVI [52], as well as a video editing approach Pix2Video [7]. Since PCNet requires identifying all objects within a scene, we are only able to evaluate it on Kubric datasets. Amodal segmentation masks for all methods are obtained by thresholding their predicted frames. For VAS, we also compare against EoRaS [21], with its pre-trained checkpoints on MOVi-B and MOVi-D. We utilize PSNR, SSIM [92], and LPIPS [114] to evaluate image alignment with ground-truth reference frames, mIoU for amodal mask alignment, and CLIP-T [20] and FVD [83] to assess cross-frame consistency. Further details on metrics and baselines are provided in *supplementary materials*.

Table 2. **User Study.**

Method	CQ (\uparrow)	CC (\uparrow)	CP (\uparrow)
Pix2Video	2.20	2.44	2.13
pix2gestalt	2.88	2.44	2.63
E ² FGVI	2.60	2.95	2.53
Ours	4.65	4.63	4.64

Table 3. **VAS results.**

Method	Zero-shot	MOVi-B	MOVi-D
E ² FGVI	✓	41.9	31.2
P2G(Top-1)	✓	56.4	48.3
P2G(Top-3)	✓	57.2	48.9
Ours(Top-1)	✓	73.1	56.6
Ours(Top-3)	✓	77.8	61.3
EoRaS	×	75.8	69.4

Results We present VAC comparison results in Tab. 1 and qualitative examples in Fig. 4, with user study summarized in Tab. 2. VAS comparison results on MOVi-B and MOVi-D are shown in Tab. 3. Our method outperforms all baselines on all VAC benchmarks and user studies from 36 participants in Content Quality (CQ), Content Consistency (CC),

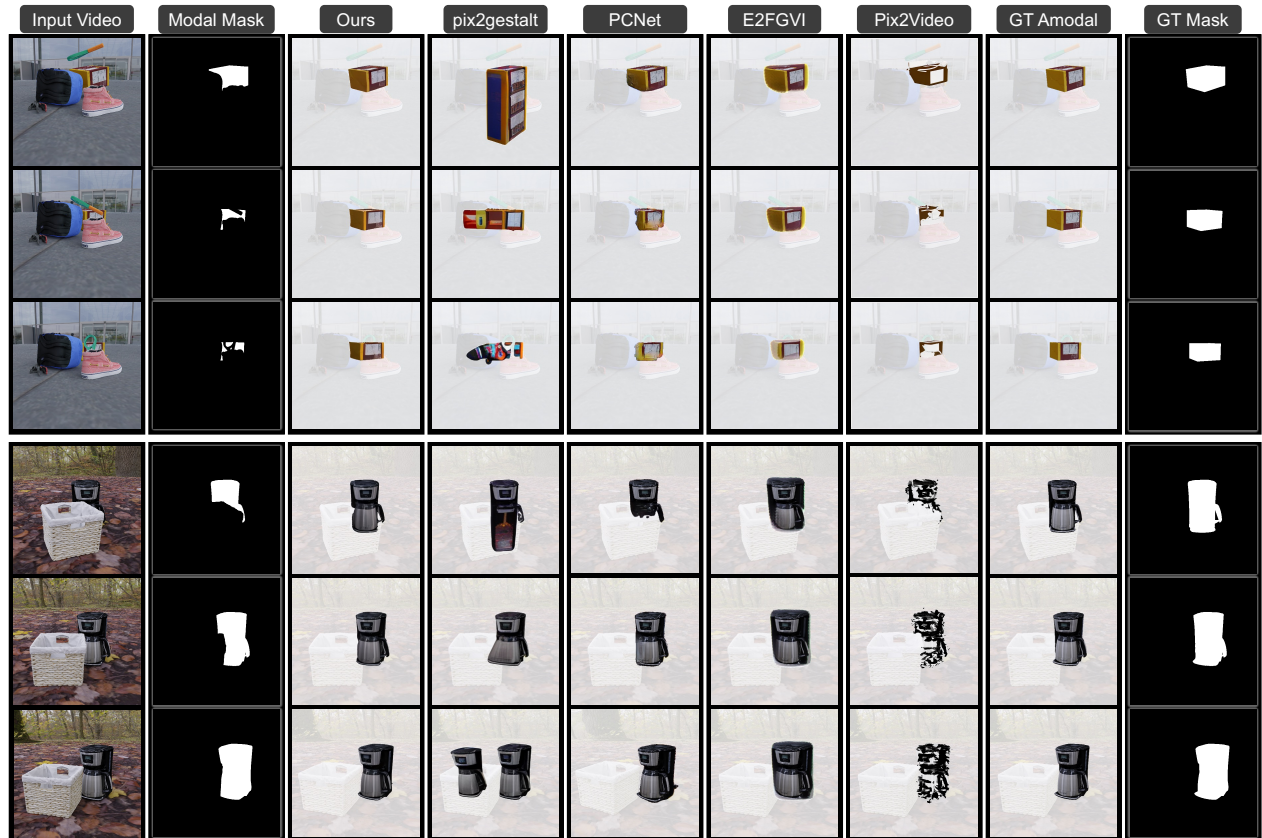


Figure 4. **Qualitative comparison on Kubric** [26]. The first example is from Kubric-Dynamic and the second from Kubric-Static. Our method achieves better consistency and can effectively extract information from nearby frames to handle highly occluded scenarios.

and Content Plausibility (CP) with significantly better content quality and consistency. On VAS benchmarks, our method outperforms all zero-shot baselines and even outperforms EoRaS [21] trained on MOVi-B. From visualized results, E²FGVI [52] and Pix2Video [7] show good consistency across frames but fail to generate reasonable amodal content. PCNet [113] and pix2gestalt [67] generate plausible content in a single frame but struggle with cross-frame consistency as image-level models and fail in highly occluded scenarios, as shown in the first example in Fig. 4.

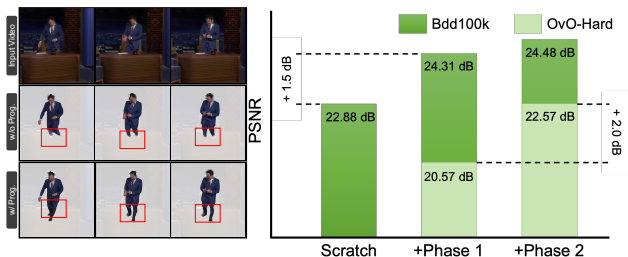


Figure 5. **Ablation study.** We test our model’s performance w/ and w/o progressive training on OvO-Hard and Bdd100k test set.

5.2. Ablation Study

To assess the effectiveness of our progressive training paradigm, we conduct an ablation study in Fig. 5. The qualitative results show that models trained progressively synthesize more complete and coherent content. Additionally, we quantitatively benchmark performance on Bdd100k and OvO-Hard in Fig. 5. The *Phase 1* and *Phase 2* correspond to the progressive training stages in Sec. 4.2. For Bdd100k, *Scratch* refers to training without progressive learning, inheriting weights directly from SVD. In contrast, *Phase 1* and *Phase 2* significantly benefit its performance by building upon weights from corresponding phases on OvO.

5.3. Object Reconstruction

Setup We demonstrate that VAC significantly enhances object reconstruction, particularly in challenging occluded scenarios. We benchmark our approach on a Compositional-GSO dataset [18] with 20 scenes, leveraging NeRF2Mesh [80] to reconstruct objects from synthesized images. Further details are in *supplementary materials*.

Results We compare 3D reconstruction results using only the visible parts of objects against those generated by our model, pix2gestalt [67], and E²FGVI [52]. For refer-

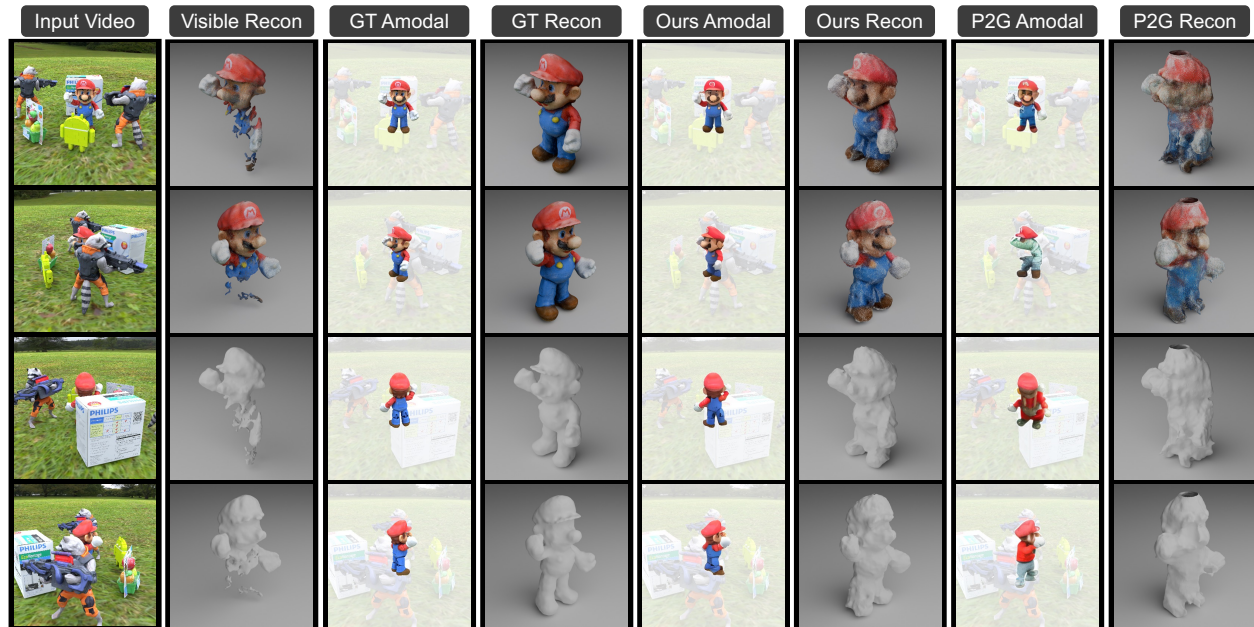


Figure 6. **Visualized comparison on reconstruction.** Our method is capable of reconstructing more complete and higher-quality textured mesh, further demonstrating the consistency of our synthesized results. ‘P2G’ denotes pix2gestalt [67].

Table 4. **Quantitative comparison on object reconstruction.** Our method provides consistent amodal objects that lead to better geometry compared with baselines.

Method	CD (\downarrow)	F-Score (\uparrow)	NC (\uparrow)
E ² FGVI	7.57	22.34	56.16
Visible	4.39	34.86	65.99
pix2gestalt	1.97	45.30	75.04
Ours	1.26	57.71	81.09
GT Amodal	1.05	66.01	84.41

ence, we also include reconstructions using GT amodal images. We utilize Chamfer Distance (CD), F-Score, and Normal Consistency (NC) as metrics, with quantitative results in Tab. 4 and qualitative comparison in Fig. 6. Our method showcases significantly better reconstruction quality, closely aligning with GT. The ‘Visible’ baseline lacks information in occluded areas, leading to significant missing parts of the object during reconstruction. While pix2gestalt [67] can synthesize content in occluded regions, it fails to guarantee multi-view consistency, leading to compromised reconstructions. In contrast, our method effectively synthesizes consistent multi-view images, providing a solid foundation for high-quality object reconstruction.

5.4. 6-DoF Object Pose Estimation

Setup We test if video amodal completion can improve 6-DoF object pose estimation in occluded scenarios. Given a video, we first synthesize the complete object and integrate

Table 5. **Quantitative comparison on pose estimation.** Our method predicts plausible content in occluded areas, offering additional information that improves the accuracy of pose estimation.

Method	Rot-Acc (\uparrow)	trans-Acc (\uparrow)	Rot-Err (\downarrow)	trans-Err (\downarrow)
w/o ours	26.5	11.3	41.5	67.8
w/ ours	34.7	13.8	39.1	59.1

it back into the original scene. We then compare the performance of pose estimation with and without our method, using an off-the-shelf pose estimation module POPE [22].



Figure 7. **6-DoF pose estimation on YCB-Video [97].** TACO aids accurate pose estimation by synthesizing occluded contents. **Results** We test on a total of 336 image pairs from YCB-Video [97]. From Tab. 5, incorporating our amodal prediction helps POPE to better comprehend the location, orienta-

tion, and size of occluded objects. From visualized results in Fig. 7, POPE predicts more accurate pose, especially orientation, with the help of amodal contents.

6. Conclusion

We propose **TACO** for Video Amodal Completion (VAC), leveraging the rich consistent manifolds learned by pre-trained diffusion models. For robust generalization to in-the-wild videos, we curate a scalable dataset from diverse real-world videos with multiple difficulty levels and introduce a progressive fine-tuning paradigm. We demonstrate **TACO**'s generalization capability to diverse in-the-wild videos as well as its potential to aid downstream tasks.

References

- [1] Niket Agarwal, Arslan Ali, Maciej Bala, Yogesh Balaji, Erik Barker, Tiffany Cai, Prithvijit Chattopadhyay, Yongxin Chen, Yin Cui, Yifan Ding, et al. Cosmos world foundation model platform for physical ai. *arXiv preprint arXiv:2501.03575*, 2025. 3
- [2] Ali Athar, Jonathon Luiten, Paul Voigtlaender, Tarasha Khurana, Achal Dave, Bastian Leibe, and Deva Ramanan. Burst: A benchmark for unifying object recognition, segmentation and tracking in video. In *Proceedings of Winter Conference on Applications of Computer Vision (WACV)*, 2023. 2
- [3] Max Bain, Arsha Nagrani, Gül Varol, and Andrew Zisserman. Frozen in time: A joint video and image encoder for end-to-end retrieval. In *International Conference on Computer Vision (ICCV)*, 2021. 2
- [4] Andreas Blattmann, Tim Dockhorn, Sumith Kulal, Daniel Mendelevitch, Maciej Kilian, Dominik Lorenz, Yam Levi, Zion English, Vikram Voleti, Adam Letts, et al. Stable video diffusion: Scaling latent video diffusion models to large datasets. *arXiv preprint arXiv:2311.15127*, 2023. 2, 3, 4, 5, 15
- [5] Andreas Blattmann, Robin Rombach, Huan Ling, Tim Dockhorn, Seung Wook Kim, Sanja Fidler, and Karsten Kreis. Align your latents: High-resolution video synthesis with latent diffusion models. In *Conference on Computer Vision and Pattern Recognition (CVPR)*, 2023. 3
- [6] Anthony Brohan, Noah Brown, Justice Carbajal, Yevgen Chebotar, Xi Chen, Krzysztof Choromanski, Tianli Ding, Danny Driess, Avinava Dubey, Chelsea Finn, et al. Rt-2: Vision-language-action models transfer web knowledge to robotic control. *arXiv preprint arXiv:2307.15818*, 2023. 2
- [7] Duygu Ceylan, Chun-Hao P Huang, and Niloy J Mitra. Pix2video: Video editing using image diffusion. In *International Conference on Computer Vision (ICCV)*, 2023. 6, 7
- [8] Ya-Liang Chang, Zhe Yu Liu, Kuan-Ying Lee, and Winston Hsu. Learnable gated temporal shift module for deep video inpainting. *arXiv preprint arXiv:1907.01131*, 2019. 3
- [9] Kaihua Chen, Deva Ramanan, and Tarasha Khurana. Using diffusion priors for video amodal segmentation. *arXiv preprint arXiv:2412.04623*, 2024. 3
- [10] Yixin Chen, Junfeng Ni, Nan Jiang, Yaowei Zhang, Yixin Zhu, and Siyuan Huang. Single-view 3d scene reconstruction with high-fidelity shape and texture. In *International Conference on 3D Vision (3DV)*, 2024. 2
- [11] Hsu-kuang Chiu, Jie Li, Rareş Ambruş, and Jeannette Bohg. Probabilistic 3d multi-modal, multi-object tracking for autonomous driving. In *International Conference on Robotics and Automation (ICRA)*, 2021. 2
- [12] Blender Online Community. *Blender - a 3D modelling and rendering package*. Blender Foundation, Stichting Blender Foundation, Amsterdam, 2018. 3, 15, 16
- [13] Ciprian Corneanu, Raghudeep Gadde, and Aleix M Martinez. Latentpaint: Image inpainting in latent space with diffusion models. In *Proceedings of Winter Conference on Applications of Computer Vision (WACV)*, 2024. 3
- [14] Angela Dai, Angel X Chang, Manolis Savva, Maciej Halber, Thomas Funkhouser, and Matthias Nießner. Scannet: Richly-annotated 3d reconstructions of indoor scenes. In *Conference on Computer Vision and Pattern Recognition (CVPR)*, 2017. 2, 6, 17, 18, 19, 21, 22, 23
- [15] Achal Dave, Tarasha Khurana, Pavel Tokmakov, Cordelia Schmid, and Deva Ramanan. Tao: A large-scale benchmark for tracking any object. In *European Conference on Computer Vision (ECCV)*, 2020. 2
- [16] Matt Deitke, Ruoshi Liu, Matthew Wallingford, Huong Ngo, Oscar Michel, Aditya Kusupati, Alan Fan, Christian Laforte, Vikram Voleti, Samir Yitzhak Gadre, et al. Objaverse-xl: A universe of 10m+ 3d objects. *Advances in Neural Information Processing Systems (NeurIPS)*, 2023. 14
- [17] Matt Deitke, Dustin Schwenk, Jordi Salvador, Luca Weihs, Oscar Michel, Eli VanderBilt, Ludwig Schmidt, Kiana Ehsani, Aniruddha Kembhavi, and Ali Farhadi. Objaverse: A universe of annotated 3d objects. In *Conference on Computer Vision and Pattern Recognition (CVPR)*, 2023. 14, 15
- [18] Laura Downs, Anthony Francis, Nate Koenig, Brandon Kinman, Ryan Hickman, Krista Reymann, Thomas B McHugh, and Vincent Vanhoucke. Google scanned objects: A high-quality dataset of 3d scanned household items. In *International Conference on Robotics and Automation (ICRA)*, 2022. 6, 7, 16
- [19] Frederik Ebert, Yanlai Yang, Karl Schmeckpeper, Bernadette Bucher, Georgios Georgakis, Kostas Daniilidis, Chelsea Finn, and Sergey Levine. Bridge data: Boosting generalization of robotic skills with cross-domain datasets. *arXiv preprint arXiv:2109.13396*, 2021. 2, 6, 17, 18, 19, 24, 25, 26
- [20] Patrick Esser, Johnathan Chiu, Parmida Atighehchian, Jonathan Granskog, and Anastasis Germanidis. Structure and content-guided video synthesis with diffusion models. In *International Conference on Computer Vision (ICCV)*, 2023. 6
- [21] Ke Fan, Jingshi Lei, Xuelin Qian, Miaopeng Yu, Tianjun Xiao, Tong He, Zheng Zhang, and Yanwei Fu. Rethinking amodal video segmentation from learning supervised signals with object-centric representation. In *International Conference on Computer Vision (ICCV)*, 2023. 2, 6, 7

- [22] Zhiwen Fan, Panwang Pan, Peihao Wang, Yifan Jiang, De-
jia Xu, and Zhangyang Wang. Pope: 6-dof promptable pose
estimation of any object in any scene with one reference. In
*Conference on Computer Vision and Pattern Recognition
(CVPR)*, 2024. 8
- [23] Patrick Follmann, Rebecca König, Philipp Härtinger,
Michael Klostermann, and Tobias Böttger. Learning to
see the invisible: End-to-end trainable amodal instance seg-
mentation. In *Proceedings of Winter Conference on Appli-
cations of Computer Vision (WACV)*, 2019. 3
- [24] Chen Gao, Ayush Saraf, Jia-Bin Huang, and Johannes
Kopf. Flow-edge guided video completion. In *European
Conference on Computer Vision (ECCV)*, 2020. 2, 3
- [25] Songwei Ge, Seungjun Nah, Guilin Liu, Tyler Poon, An-
drew Tao, Bryan Catanzaro, David Jacobs, Jia-Bin Huang,
Ming-Yu Liu, and Yogesh Balaji. Preserve your own cor-
relation: A noise prior for video diffusion models. In *Inter-
national Conference on Computer Vision (ICCV)*, 2023.
3
- [26] Klaus Greff, Francois Belletti, Lucas Beyer, Carl Doersch,
Yilun Du, Daniel Duckworth, David J Fleet, Dan Gnanapra-
gasam, Florian Golemo, Charles Herrmann, et al. Kubric:
A scalable dataset generator. In *Conference on Computer
Vision and Pattern Recognition (CVPR)*, 2022. 6, 7, 16
- [27] Ming Gui, Johannes S Fischer, Ulrich Prestel, Pingchuan
Ma, Dmytro Kotovenko, Olga Grebenkova, Stefan Andreas
Baumann, Vincent Tao Hu, and Björn Ommer. Depthfm:
Fast monocular depth estimation with flow matching. *arXiv
preprint arXiv:2403.13788*, 2024. 3
- [28] Yuwei Guo, Ceyuan Yang, Anyi Rao, Zhengyang Liang,
Yaohui Wang, Yu Qiao, Maneesh Agrawala, Dahua Lin,
and Bo Dai. Animatediff: Animate your personalized text-
to-image diffusion models without specific tuning. In *Inter-
national Conference on Learning Representations (ICLR)*,
2024. 2, 3
- [29] Jonathan Ho, Ajay Jain, and Pieter Abbeel. Denoising dif-
fusion probabilistic models. *Advances in Neural Informa-
tion Processing Systems (NeurIPS)*, 2020. 4
- [30] Jonathan Ho, William Chan, Chitwan Saharia, Jay Whang,
Ruiqi Gao, Alexey Gritsenko, Diederik P Kingma, Ben
Poole, Mohammad Norouzi, David J Fleet, et al. Imagen
video: High definition video generation with diffusion
models. *arXiv preprint arXiv:2210.02303*, 2022. 3
- [31] Sebastian Höfer, Kostas Bekris, Ankur Handa, Juan Camilo
Gamboa, Melissa Mozifian, Florian Golemo, Chris Atke-
son, Dieter Fox, Ken Goldberg, John Leonard, et al. Sim2real
in robotics and automation: Applications and
challenges. *IEEE transactions on automation science and
engineering*, 18(2):398–400, 2021. 3
- [32] Wenyi Hong, Ming Ding, Wendi Zheng, Xinghan Liu,
and Jie Tang. Cogvideo: Large-scale pretraining for
text-to-video generation via transformers. *arXiv preprint
arXiv:2205.15868*, 2022. 2, 3, 5
- [33] Cheng-Yen Hsieh, Tarasha Khurana, Achal Dave, and Deva
Ramanan. Tracking any object amodally. *arXiv preprint
arXiv:2312.12433*, 2023. 2
- [34] Wenbo Hu, Xiangjun Gao, Xiaoyu Li, Sijie Zhao, Xi-
aodong Cun, Yong Zhang, Long Quan, and Ying Shan.
Depthcrafter: Generating consistent long depth sequences
for open-world videos. *arXiv preprint arXiv:2409.02095*,
2024. 3, 5
- [35] Yuan-Ting Hu, Hong-Shuo Chen, Kexin Hui, Jia-Bin
Huang, and Alexander G Schwing. Sail-vos: Semantic
amodal instance level video object segmentation—a syn-
thetic dataset and baselines. In *Conference on Computer
Vision and Pattern Recognition (CVPR)*, 2019. 2, 3
- [36] Yuan-Ting Hu, Heng Wang, Nicolas Ballas, Kristen Grau-
man, and Alexander G Schwing. Proposal-based video
completion. In *European Conference on Computer Vision
(ECCV)*, 2020. 3
- [37] Xuan Ju, Xian Liu, Xintao Wang, Yuxuan Bian, Ying Shan,
and Qiang Xu. Brushnet: A plug-and-play image inpaint-
ing model with decomposed dual-branch diffusion. In *Eu-
ropean Conference on Computer Vision (ECCV)*, 2024. 2
- [38] Abhishek Kar, Shubham Tulsiani, Joao Carreira, and Jiten-
dra Malik. Amodal completion and size constancy in natu-
ral scenes. In *International Conference on Computer Vision
(ICCV)*, 2015. 2
- [39] Tero Karras, Miika Aittala, Timo Aila, and Samuli Laine.
Elucidating the design space of diffusion-based generative
models. In *Advances in Neural Information Processing Sys-
tems (NeurIPS)*, 2022. 4, 15
- [40] Bingxin Ke, Anton Obukhov, Shengyu Huang, Nando Met-
zger, Rodrigo Caye Daudt, and Konrad Schindler. Re-
purposing diffusion-based image generators for monocular
depth estimation. In *Conference on Computer Vision and
Pattern Recognition (CVPR)*, 2024. 3
- [41] Lei Ke, Yu-Wing Tai, and Chi-Keung Tang. Deep
occlusion-aware instance segmentation with overlapping
bilayers. In *Conference on Computer Vision and Pattern
Recognition (CVPR)*, 2021. 2
- [42] Lei Ke, Yu-Wing Tai, and Chi-Keung Tang. Occlusion-
aware video object inpainting. In *International Conference
on Computer Vision (ICCV)*, 2021. 2
- [43] Dahun Kim, Sanghyun Woo, Joon-Young Lee, and In So
Kweon. Deep video inpainting. In *Conference on Computer
Vision and Pattern Recognition (CVPR)*, 2019. 2
- [44] Diederik P Kingma. Auto-encoding variational bayes.
arXiv preprint arXiv:1312.6114, 2013. 5
- [45] Alexander Kirillov, Eric Mintun, Nikhila Ravi, Hanzi
Mao, Chloe Rolland, Laura Gustafson, Tete Xiao, Spencer
Whitehead, Alexander C Berg, Wan-Yen Lo, et al. Segment
anything. In *International Conference on Computer Vision
(ICCV)*, 2023. 3, 4, 5, 14, 15
- [46] Kurt Koffka. *Principles of Gestalt psychology*. routledge,
2013. 2
- [47] Sungho Lee, Seoung Wug Oh, DaeYeun Won, and Seon Joo
Kim. Copy-and-paste networks for deep video inpainting.
In *International Conference on Computer Vision (ICCV)*,
2019. 2, 3
- [48] Ang Li, Shanshan Zhao, Xingjun Ma, Mingming Gong,
Jianzhong Qi, Rui Zhang, Dacheng Tao, and Ramamoha-
narao Kotagiri. Short-term and long-term context aggrega-
tion network for video inpainting. In *European Conference
on Computer Vision (ECCV)*, 2020. 3

- [49] Ke Li and Jitendra Malik. Amodal instance segmentation. In *European Conference on Computer Vision (ECCV)*, 2016. 3
- [50] Puhao Li, Tengyu Liu, Yuyang Li, Muzhi Han, Haoran Geng, Shu Wang, Yixin Zhu, Song-Chun Zhu, and Siyuan Huang. Ag2manip: Learning novel manipulation skills with agent-agnostic visual and action representations. *arXiv preprint arXiv:2404.17521*, 2024. 2, 3
- [51] Ruining Li, Chuanxia Zheng, Christian Rupprecht, and Andrea Vedaldi. Puppet-master: Scaling interactive video generation as a motion prior for part-level dynamics. *arXiv preprint arXiv:2408.04631*, 2024. 3, 5, 15
- [52] Zhen Li, Cheng-Ze Lu, Jianhua Qin, Chun-Le Guo, and Ming-Ming Cheng. Towards an end-to-end framework for flow-guided video inpainting. In *Conference on Computer Vision and Pattern Recognition (CVPR)*, 2022. 2, 3, 6, 7
- [53] Junbang Liang, Ruoshi Liu, Ege Ozguroglu, Sruthi Sudhakar, Achal Dave, Pavel Tokmakov, Shuran Song, and Carl Vondrick. Dreamitate: Real-world visuomotor policy learning via video generation. *arXiv preprint arXiv:2406.16862*, 2024. 3
- [54] Huan Ling, David Acuna, Karsten Kreis, Seung Wook Kim, and Sanja Fidler. Variational amodal object completion. In *Advances in Neural Information Processing Systems (NeurIPS)*, 2020. 2
- [55] Fangfu Liu, Wenqiang Sun, Hanyang Wang, Yikai Wang, Haowen Sun, Junliang Ye, Jun Zhang, and Yueqi Duan. Reconx: Reconstruct any scene from sparse views with video diffusion model. *arXiv preprint arXiv:2408.16767*, 2024. 3
- [56] Rui Liu, Hanming Deng, Yangyi Huang, Xiaoyu Shi, Lewei Lu, Wenxiu Sun, Xiaogang Wang, Jifeng Dai, and Hongsheng Li. Fuseformer: Fusing fine-grained information in transformers for video inpainting. In *International Conference on Computer Vision (ICCV)*, 2021. 3
- [57] Ruoshi Liu, Rundi Wu, Basile Van Hoorick, Pavel Tokmakov, Sergey Zakharov, and Carl Vondrick. Zero-1-to-3: Zero-shot one image to 3d object. In *International Conference on Computer Vision (ICCV)*, 2023. 3
- [58] Yu Liu, Baoxiong Jia, Yixin Chen, and Siyuan Huang. Slotlifter: Slot-guided feature lifting for learning object-centric radiance fields. In *European Conference on Computer Vision (ECCV)*, 2024. 2
- [59] Yu Liu, Baoxiong Jia, Ruijie Lu, Junfeng Ni, Song-Chun Zhu, and Siyuan Huang. Building interactable replicas of complex articulated objects via gaussian splatting. *arXiv preprint arXiv:2502.19459*, 2025. 2
- [60] Francesco Locatello, Dirk Weissenborn, Thomas Unterthiner, Aravindh Mahendran, Georg Heigold, Jakob Uszkoreit, Alexey Dosovitskiy, and Thomas Kipf. Object-centric learning with slot attention. *Advances in Neural Information Processing Systems (NeurIPS)*, 2020. 2
- [61] Guanxing Lu, Shiyi Zhang, Ziwei Wang, Changliu Liu, Jiwen Lu, and Yansong Tang. Manigaussian: Dynamic gaussian splatting for multi-task robotic manipulation. In *European Conference on Computer Vision (ECCV)*, 2024. 2
- [62] Ruijie Lu, Yixin Chen, Junfeng Ni, Baoxiong Jia, Yu Liu, Diwen Wan, Gang Zeng, and Siyuan Huang. Mo-vis: Enhancing multi-object novel view synthesis for indoor scenes. *arXiv preprint arXiv:2412.11457*, 2024. 3
- [63] Andreas Lugmayr, Martin Danelljan, Andres Romero, Fisher Yu, Radu Timofte, and Luc Van Gool. Repaint: Inpainting using denoising diffusion probabilistic models. In *Conference on Computer Vision and Pattern Recognition (CVPR)*, 2022. 2, 3
- [64] Xinzhu Ma, Zhihui Wang, Haojie Li, Pengbo Zhang, Wanli Ouyang, and Xin Fan. Accurate monocular 3d object detection via color-embedded 3d reconstruction for autonomous driving. In *International Conference on Computer Vision (ICCV)*, 2019. 2
- [65] Junfeng Ni, Yixin Chen, Bohan Jing, Nan Jiang, Bin Wang, Bo Dai, Puhao Li, Yixin Zhu, Song-Chun Zhu, and Siyuan Huang. Phyrecon: Physically plausible neural scene reconstruction. In *Advances in Neural Information Processing Systems (NeurIPS)*, 2024. 2
- [66] Junfeng Ni, Yu Liu, Ruijie Lu, Zirui Zhou, Song-Chun Zhu, Yixin Chen, and Siyuan Huang. Decompositional neural scene reconstruction with generative diffusion prior. In *Conference on Computer Vision and Pattern Recognition (CVPR)*, 2025. 2
- [67] Ege Ozguroglu, Ruoshi Liu, Dídac Surís, Dian Chen, Achal Dave, Pavel Tokmakov, and Carl Vondrick. pix2gestalt: Amodal segmentation by synthesizing wholes. In *Conference on Computer Vision and Pattern Recognition (CVPR)*, 2024. 2, 3, 6, 7, 8, 15, 16, 18
- [68] Lu Qi, Li Jiang, Shu Liu, Xiaoyong Shen, and Jiaya Jia. Amodal instance segmentation with kins dataset. In *Conference on Computer Vision and Pattern Recognition (CVPR)*, 2019. 2
- [69] Weize Quan, Jiayi Chen, Yanli Liu, Dong-Ming Yan, and Peter Wonka. Deep learning-based image and video inpainting: A survey. *International Journal of Computer Vision (IJCV)*, 132(7):2367–2400, 2024. 3
- [70] Alec Radford, Jong Wook Kim, Chris Hallacy, Aditya Ramesh, Gabriel Goh, Sandhini Agarwal, Girish Sastry, Amanda Askell, Pamela Mishkin, Jack Clark, et al. Learning transferable visual models from natural language supervision. In *ICML*, pages 8748–8763. PMLR, 2021. 5
- [71] Aditya Ramesh, Mikhail Pavlov, Gabriel Goh, Scott Gray, Chelsea Voss, Alec Radford, Mark Chen, and Ilya Sutskever. Zero-shot text-to-image generation. In *International Conference on Machine Learning (ICML)*, 2021. 3
- [72] Nikhila Ravi, Valentin Gabeur, Yuan-Ting Hu, Ronghang Hu, Chaitanya Ryali, Tengyu Ma, Haitham Khedr, Roman Rädle, Chloe Rolland, Laura Gustafson, et al. Sam 2: Segment anything in images and videos. *arXiv preprint arXiv:2408.00714*, 2024. 2, 3, 4, 5, 15, 17
- [73] N Dinesh Reddy, Robert Tamburo, and Srinivasa G Narasimhan. Walt: Watch and learn 2d amodal representation from time-lapse imagery. In *Conference on Computer Vision and Pattern Recognition (CVPR)*, 2022. 2
- [74] Tianhe Ren, Shilong Liu, Ailing Zeng, Jing Lin, Kunchang Li, He Cao, Jiayu Chen, Xinyu Huang, Yukang Chen, Feng Yan, et al. Grounded sam: Assembling open-world models for diverse visual tasks. *arXiv preprint arXiv:2401.14159*, 2024. 3, 4

- [75] Robin Rombach, Andreas Blattmann, Dominik Lorenz, Patrick Esser, and Björn Ommer. High-resolution image synthesis with latent diffusion models. In *Conference on Computer Vision and Pattern Recognition (CVPR)*, 2022. 2, 3
- [76] Chitwan Saharia, William Chan, Saurabh Saxena, Lala Li, Jay Whang, Emily L Denton, Kamyar Ghasemipour, Raphael Gontijo Lopes, Burcu Karagol Ayan, Tim Salimans, et al. Photorealistic text-to-image diffusion models with deep language understanding. *Advances in Neural Information Processing Systems (NeurIPS)*, 2022. 3
- [77] Jiahao Shao, Yuanbo Yang, Hongyu Zhou, Youmin Zhang, Yujun Shen, Matteo Poggi, and Yiyi Liao. Learning temporally consistent video depth from video diffusion priors. *arXiv preprint arXiv:2406.01493*, 2024. 3, 5
- [78] Uriel Singer, Adam Polyak, Thomas Hayes, Xi Yin, Jie An, Songyang Zhang, Qiyuan Hu, Harry Yang, Oron Ashual, Oran Gafni, et al. Make-a-video: Text-to-video generation without text-video data. *arXiv preprint arXiv:2209.14792*, 2022. 3
- [79] Jiaming Song, Chenlin Meng, and Stefano Ermon. Denoising diffusion implicit models. In *International Conference on Learning Representations (ICLR)*, 2020. 4
- [80] Jiayang Tang, Hang Zhou, Xiaokang Chen, Tianshu Hu, Errui Ding, Jingdong Wang, and Gang Zeng. Delicate textured mesh recovery from nerf via adaptive surface refinement. In *International Conference on Computer Vision (ICCV)*, 2023. 7, 16
- [81] Jiayang Tang, Ruijie Lu, Xiaokang Chen, Xiang Wen, Gang Zeng, and Ziwei Liu. Intex: Interactive text-to-texture synthesis via unified depth-aware inpainting. *arXiv preprint arXiv:2403.11878*, 2024. 2
- [82] Octo Model Team, Dibya Ghosh, Homer Walke, Karl Pertsch, Kevin Black, Oier Mees, Sudeep Dasari, Joey Hejna, Tobias Kreiman, Charles Xu, et al. Octo: An open-source generalist robot policy. *arXiv preprint arXiv:2405.12213*, 2024. 2
- [83] Thomas Unterthiner, Sjoerd Van Steenkiste, Karol Kurach, Raphael Marinier, Marcin Michalski, and Sylvain Gelly. Towards accurate generative models of video: A new metric & challenges. *arXiv preprint arXiv:1812.01717*, 2018. 6
- [84] Basile Van Hoorick, Pavel Tokmakov, Simon Stent, Jie Li, and Carl Vondrick. Tracking through containers and occluders in the wild. In *Conference on Computer Vision and Pattern Recognition (CVPR)*, 2023. 2
- [85] Basile Van Hoorick, Rundi Wu, Ege Ozguroglu, Kyle Sargent, Ruoshi Liu, Pavel Tokmakov, Achal Dave, Changxi Zheng, and Carl Vondrick. Generative camera dolly: Extreme monocular dynamic novel view synthesis. *arXiv preprint arXiv:2405.14868*, 2024. 3, 5, 15
- [86] Vikram Voleti, Chun-Han Yao, Mark Boss, Adam Letts, David Pankratz, Dmitry Tochilkin, Christian Laforte, Robin Rombach, and Varun Jampani. Sv3d: Novel multi-view synthesis and 3d generation from a single image using latent video diffusion. In *European Conference on Computer Vision (ECCV)*, 2025. 3
- [87] Johan Wagemans, James H Elder, Michael Kubovy, Stephen E Palmer, Mary A Peterson, Manish Singh, and Rüdiger Von der Heydt. A century of gestalt psychology in visual perception: I. perceptual grouping and figure-ground organization. *Psychological bulletin*, 138(6):1172, 2012. 2
- [88] Homer Rich Walke, Kevin Black, Tony Z Zhao, Quan Vuong, Chongyi Zheng, Philippe Hansen-Estruch, Andre Wang He, Vivek Myers, Moo Jin Kim, Max Du, et al. Bridgedata v2: A dataset for robot learning at scale. In *Conference on Robot Learning (CoRL)*, 2023. 2, 6, 17, 18, 19, 24, 25, 26
- [89] Diwen Wan, Ruijie Lu, and Gang Zeng. Superpoint gaussian splatting for real-time high-fidelity dynamic scene reconstruction. *arXiv preprint arXiv:2406.03697*, 2024. 2
- [90] Qi Wang, Ruijie Lu, Xudong Xu, Jingbo Wang, Michael Yu Wang, Bo Dai, Gang Zeng, and Dan Xu. Roomtex: Texturing compositional indoor scenes via iterative inpainting. In *European Conference on Computer Vision (ECCV)*, 2024.
- [91] Shuzhe Wang, Vincent Leroy, Yohann Cabon, Boris Chidlovskii, and Jerome Revaud. Dust3r: Geometric 3d vision made easy. In *Conference on Computer Vision and Pattern Recognition (CVPR)*, 2024. 2
- [92] Zhou Wang, Alan C Bovik, Hamid R Sheikh, and Eero P Simoncelli. Image quality assessment: from error visibility to structural similarity. *Transactions on Image Processing (TIP)*, 13(4):600–612, 2004. 6
- [93] Max Wertheimer. Experimentelle studien uber das sehen von bewegung. *Zeitschrift fur psychologie*, 61:161–165, 1912. 2
- [94] Max Wertheimer. Untersuchungen zur lehre von der gestalt. *Gestalt Theory*, 39(1):79–89, 2017. 2
- [95] Jianzong Wu, Xiangtai Li, Chenyang Si, Shangchen Zhou, Jingkang Yang, Jiangning Zhang, Yining Li, Kai Chen, Yunhai Tong, Ziwei Liu, et al. Towards language-driven video inpainting via multimodal large language models. In *Conference on Computer Vision and Pattern Recognition (CVPR)*, 2024. 3
- [96] Fanbo Xiang, Yuzhe Qin, Kaichun Mo, Yikuan Xia, Hao Zhu, Fangchen Liu, Minghua Liu, Hanxiao Jiang, Yifu Yuan, He Wang, et al. Sapien: A simulated part-based interactive environment. In *Conference on Computer Vision and Pattern Recognition (CVPR)*, 2020. 3
- [97] Yu Xiang, Tanner Schmidt, Venkatraman Narayanan, and Dieter Fox. Posecnn: A convolutional neural network for 6d object pose estimation in cluttered scenes. *arXiv preprint arXiv:1711.00199*, 2017. 8, 17, 18, 19, 27, 28
- [98] Yiming Xie, Chun-Han Yao, Vikram Voleti, Huaizu Jiang, and Varun Jampani. Sv4d: Dynamic 3d content generation with multi-frame and multi-view consistency. *arXiv preprint arXiv:2407.17470*, 2024. 3
- [99] Jinbo Xing, Menghan Xia, Yong Zhang, Haoxin Chen, Wangbo Yu, Hanyuan Liu, Gongye Liu, Xintao Wang, Ying Shan, and Tien-Tsin Wong. Dynamicrafter: Animating open-domain images with video diffusion priors. In *European Conference on Computer Vision (ECCV)*, 2025. 2, 3, 5
- [100] Katherine Xu, Lingzhi Zhang, and Jianbo Shi. Amodal completion via progressive mixed context diffusion. In

- Conference on Computer Vision and Pattern Recognition (CVPR)*, 2024. 2
- [101] Ning Xu, Linjie Yang, Yuchen Fan, Dingcheng Yue, Yuchen Liang, Jianchao Yang, and Thomas Huang. Youtube-vos: A large-scale video object segmentation benchmark. *arXiv preprint arXiv:1809.03327*, 2018. 6, 17, 18, 20, 29, 30
- [102] Rui Xu, Xiaoxiao Li, Bolei Zhou, and Chen Change Loy. Deep flow-guided video inpainting. In *Conference on Computer Vision and Pattern Recognition (CVPR)*, 2019. 3
- [103] Lihe Yang, Bingyi Kang, Zilong Huang, Xiaogang Xu, Jiashi Feng, and Hengshuang Zhao. Depth anything: Unleashing the power of large-scale unlabeled data. In *Conference on Computer Vision and Pattern Recognition (CVPR)*, 2024. 3
- [104] Zhuoyi Yang, Jiayan Teng, Wendi Zheng, Ming Ding, Shiyu Huang, Jiazheng Xu, Yuanming Yang, Wenyi Hong, Xiaohan Zhang, Guanyu Feng, et al. Cogvideox: Text-to-video diffusion models with an expert transformer. *arXiv preprint arXiv:2408.06072*, 2024. 3
- [105] Jian Yao, Yuxin Hong, Chiyu Wang, Tianjun Xiao, Tong He, Francesco Locatello, David P Wipf, Yanwei Fu, and Zheng Zhang. Self-supervised amodal video object segmentation. In *Advances in Neural Information Processing Systems (NeurIPS)*, 2022. 2
- [106] Chandan Yeshwanth, Yueh-Cheng Liu, Matthias Nießner, and Angela Dai. Scannet++: A high-fidelity dataset of 3d indoor scenes. In *International Conference on Computer Vision (ICCV)*, 2023. 2, 6, 17, 18, 19, 21, 22, 23
- [107] Fisher Yu, Haofeng Chen, Xin Wang, Wenqi Xian, Yingying Chen, Fangchen Liu, Vashisht Madhavan, and Trevor Darrell. Bdd100k: A diverse driving dataset for heterogeneous multitask learning. In *Conference on Computer Vision and Pattern Recognition (CVPR)*, 2020. 3, 5, 6, 15, 18, 20
- [108] Wangbo Yu, Jinbo Xing, Li Yuan, Wenbo Hu, Xiaoyu Li, Zhipeng Huang, Xiangjun Gao, Tien-Tsin Wong, Ying Shan, and Yonghong Tian. Viewcrafter: Taming video diffusion models for high-fidelity novel view synthesis. *arXiv preprint arXiv:2409.02048*, 2024. 3
- [109] Xianggang Yu, Mutian Xu, Yidan Zhang, Haolin Liu, Chongjie Ye, Yushuang Wu, Zizheng Yan, Chenming Zhu, Zhangyang Xiong, Tianyou Liang, et al. Mvimnet: A large-scale dataset of multi-view images. In *Conference on Computer Vision and Pattern Recognition (CVPR)*, 2023. 3, 5, 15
- [110] Zehao Yu, Songyou Peng, Michael Niemeyer, Torsten Sattler, and Andreas Geiger. Monosdf: Exploring monocular geometric cues for neural implicit surface reconstruction. In *Advances in Neural Information Processing Systems (NeurIPS)*, 2022. 2
- [111] Yanhong Zeng, Jianlong Fu, and Hongyang Chao. Learning joint spatial-temporal transformations for video inpainting. In *European Conference on Computer Vision (ECCV)*, 2020. 2
- [112] Guanqi Zhan, Chuanxia Zheng, Weidi Xie, and Andrew Zisserman. Amodal ground truth and completion in the wild. In *Conference on Computer Vision and Pattern Recognition (CVPR)*, 2024. 2
- [113] Xiaohang Zhan, Xingang Pan, Bo Dai, Ziwei Liu, Dahua Lin, and Chen Change Loy. Self-supervised scene de-occlusion. In *Conference on Computer Vision and Pattern Recognition (CVPR)*, 2020. 6, 7
- [114] Richard Zhang, Phillip Isola, Alexei A Efros, Eli Shechtman, and Oliver Wang. The unreasonable effectiveness of deep features as a perceptual metric. In *Conference on Computer Vision and Pattern Recognition (CVPR)*, 2018. 6
- [115] Zhixing Zhang, Bichen Wu, Xiaoyan Wang, Yaqiao Luo, Luxin Zhang, Yinan Zhao, Peter Vajda, Dimitris Metaxas, and Licheng Yu Avid. Any-length video inpainting with diffusion model. In *Conference on Computer Vision and Pattern Recognition (CVPR)*, 2024. 3
- [116] Yan Zhu, Yuandong Tian, Dimitris Metaxas, and Piotr Dollár. Semantic amodal segmentation. In *Conference on Computer Vision and Pattern Recognition (CVPR)*, 2017. 2
- [117] Yifeng Zhu, Abhishek Joshi, Peter Stone, and Yuke Zhu. Viola: Imitation learning for vision-based manipulation with object proposal priors. In *Conference on Robot Learning*, 2023. 2
- [118] Qi Zuo, Xiaodong Gu, Lingteng Qiu, Yuan Dong, Zhengyi Zhao, Weihao Yuan, Rui Peng, Siyu Zhu, Zilong Dong, Liefeng Bo, et al. Videomv: Consistent multi-view generation based on large video generative model. *arXiv preprint arXiv:2403.12010*, 2024. 3

TACO: Taming Diffusion for in-the-wild Video Amodal Completion

Supplementary Material

We provide details on data curation, implementation, additional qualitative results, and a discussion of limitations in *supplementary materials*. We strongly recommend exploring the local website included in *supplementary materials* for more intuitive visualizations.

A. Data Curation Details

In this section, we elaborate on the details of how we curate the Object-video-Overlay (OvO) dataset, including how to overlay occluders consistently throughout the video in Appendix A.1, how we apply image transformation techniques to augment our dataset with image-level datasets in Appendix A.2, and other curation details in Appendix A.3.

A.1. Overlay Occluders Consistently

To ensure consistent occlusions, it is crucial to maintain continuous change in the occluders’ properties across video frames. This includes the occluders’ position, \mathbf{p} , which specifies their position, and scale, \mathbf{s} , which determines their size. We employ two heuristic strategies in OvO-Easy and OvO-Hard dataset to generate occlusions.

OvO-Easy Occluders are selected from Objaverse [16, 17] and SA-1B [45]. Appropriate occlusion positions are identified for the first and last frames of the video. The occlusion rate, defined as the ratio of the occluded area to the total area of the object, is constrained to lie between 0.3 and 0.7 in both the first and last frames. For the intermediate frame i , the occlusion position \mathbf{p}_i and scale \mathbf{s}_i are determined through linear interpolation, ensuring smooth transitions:

$$\mathbf{p}_i = \frac{i}{N} \cdot (\mathbf{p}_{\text{ed}} - \mathbf{p}_{\text{st}}) + \mathbf{p}_{\text{st}}, \quad \mathbf{s}_i = \frac{i}{N} \cdot (\mathbf{s}_{\text{ed}} - \mathbf{s}_{\text{st}}) + \mathbf{s}_{\text{st}}, \quad (\text{S.5})$$

where $\mathbf{p}_{\text{st}}, \mathbf{s}_{\text{st}}, \mathbf{p}_{\text{ed}}, \mathbf{s}_{\text{ed}}$ denotes the occlusion position and scale in the first and last frame, and N stands for the total frame number. An example is illustrated in Fig. S.8. Apart from a relatively low occlusion rate, some objects are fully visible in intermediate frames.

OvO-Hard In contrast, OvO-Hard begins by selecting an initial occlusion position \mathbf{p}_{st} and scale \mathbf{s}_{st} in the first frame. The position and size of the occluder are then dynamically adjusted throughout the video, guided by changes in the bounding box of the occluded object:

$$\mathbf{p}_i = \mathbf{c}_i - \mathbf{c}_{\text{st}} + \mathbf{p}_{\text{st}}, \quad \mathbf{s}_i = \max\left(\frac{\mathbf{h}_i}{\mathbf{h}_{\text{st}}}, \frac{\mathbf{w}_i}{\mathbf{w}_{\text{st}}}\right)^{1/3} \cdot \mathbf{s}_{\text{st}}, \quad (\text{S.6})$$

where \mathbf{c}_{st} and \mathbf{c}_i stands for the center of the bounding box in the initial frame and frame i , $\mathbf{h}_i, \mathbf{w}_i, \mathbf{h}_{\text{st}},$ and \mathbf{w}_{st} stands for the height and width of the i -th frame and the initial frame. In OvO-Hard, we also apply image feathering techniques to blend the occluder more naturally into the image. The occlusion rate of the initial frame is constrained to lie between 0.4 and 0.8.

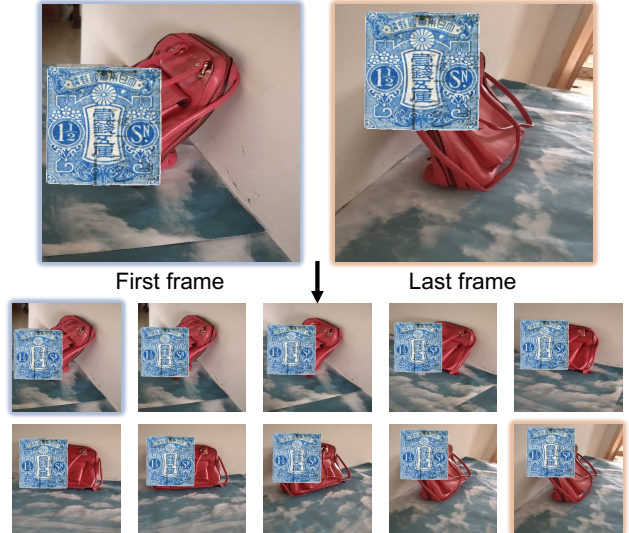


Figure S.8. **Illustration on consistent occlusion.** In OvO-Easy, we first select a proper position and scale in the first and last frame, and then interpolate in intermediate frames. The stamp is the occluder in the example.

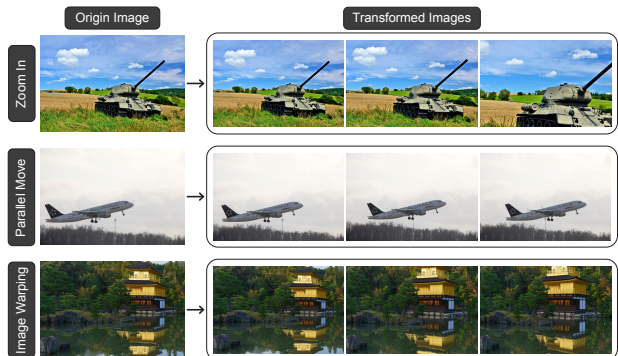


Figure S.9. **Image transformations.** We augment our OvO dataset by incorporating image-level datasets and image transformation techniques to simulate videos.

A.2. Image Transformations

In addition to introducing more severe occlusions, we further augment our dataset in OvO-Hard using the image-level dataset SA-1B [45]. Specifically, we apply three image transformation techniques: zooming, parallel moving, and image warping. An illustration of these techniques is shown in Fig. S.9. The zooming transformation is implemented by center-cropping the image, while image warping is achieved through a homography transformation. For parallel moving, we first segment the complete

foreground object using the provided annotations [45, 67]. The background area is then inpainted, after which the foreground and background are shifted in parallel to create a motion effect. For instance, in Fig. S.9, the plane visually appears to move to the right.

A.3. Other Details

In this section, we will elaborate on the data sources, the process of occluder selection, and the details of amodal check including heuristic rules and manual filtering.

Data sources To ensure the diversity of our dataset OvO, we conducted experiments using subsets of four datasets. After applying the amodal check, the final dataset consists of approximately 90K videos from MVIImgNet [109], 11K videos from SA-V [72], 10K videos from Bdd100k [107], and 24K videos from SA-1B [45]. For constructing OvO-Easy, we use data from MVIImgNet [109] and SA-V [72]. For the more challenging OvO-Hard, we further add data from Bdd100k [107] and SA-1B [45]. Additionally, we reserve approximately 1K videos as the test sets for OvO-Easy and OvO-Hard, which are used to benchmark our method against various baselines.

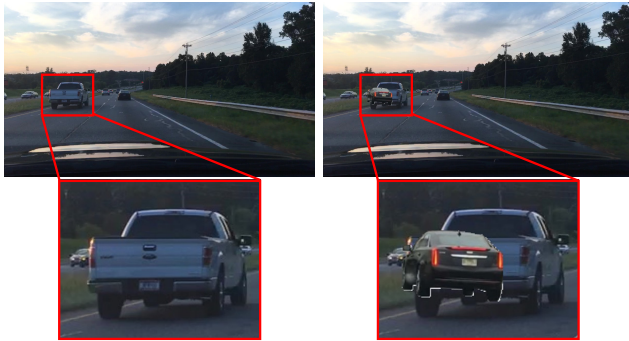


Figure S.10. **Illustration on Bdd100K occluders.** We select occluders from Bdd100K since many of the occluders in SA-1B are not applicable to the autonomous driving context.

Occluders In OvO-Easy, we select approximately 50K occluders from a subset of SA-1B [45] and around 20K occluders from a subset of Objaverse [17]. For occluders sourced from SA-1B, objects are segmented using the provided annotations, ensuring that the occluder occupies a significant portion of the image. For occluders from Objaverse, we render rotation videos consisting of 40 frames using Blender [12]. In OvO-Hard, occluders from Objaverse are excluded to enhance realism. Additionally, when curating data pairs for Bdd100k [107], we select occluders directly from Bdd100k [107] to maintain domain relevance, as many occluders from SA-1B and Objaverse are not applicable to the autonomous driving context. An example on the occluders of Bdd100k is shown in Fig. S.10.

Amodal check We apply three heuristic rules to filter out candidates likely to be incomplete, as illustrated in Fig. S.11. In the first example, the mask touches the image boundary, indicating potential incompleteness. The second example shows a mask with numerous internal holes, suggesting an inaccurate segmentation. In the third example, the pillow is positioned behind the foreground bag, failing the depth consistency check. Despite these

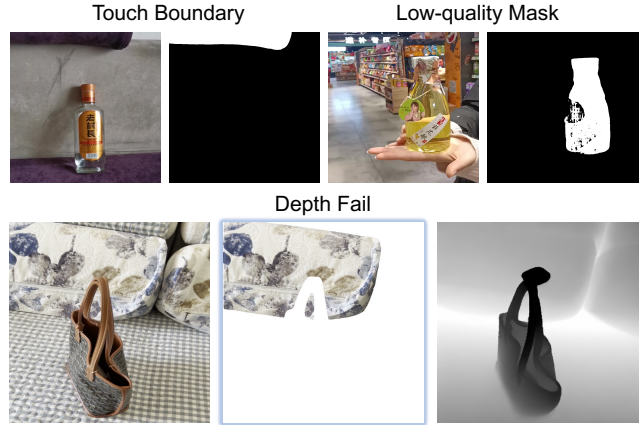


Figure S.11. **Illustration on the heuristic amodal check.** We apply three heuristic rules to check whether an object is complete.

heuristic rules, some incomplete object candidates remain. To address this, we leverage crowdsourcing to further filter out incomplete samples that have incorrectly passed the heuristic amodal check.

B. Implementation Details

In this section, we provide detailed explanations of the training and inference process in Appendix B.1, the dataset, metrics and baselines used for amodal completion and segmentation in Appendix B.2, the dataset curation and reconstruction pipeline for object reconstruction in Appendix B.3, the intermediate results for pose estimation in Appendix B.4, and details on user study in Appendix B.5.

B.1. Training and Inference Details

We trained our model on the OvO-Easy dataset for 7 epochs and continued training on the OvO-Hard dataset for another 7 epochs, resulting in a total training time of approximately 6 days using 8 NVIDIA A800 (80G) GPUs. Due to computational constraints, all input and target videos were resized to a resolution of 384×384 . The batch size per GPU was set to 4, yielding a total batch size of 32. To balance the dataset, data pairs from SA-V [72] were sampled twice per epoch. As noted in prior work [51, 85], Stable Video Diffusion (SVD)[4] is not robust to variations in resolution. To address this, we further fine-tuned the model on the Bdd100k subset for 8 epochs at a resolution of 640×384 , taking around 20 hours. This is because the typical resolution used in autonomous driving scenarios significantly differs from those in MVIImgNet[109] and SA-V [72]. We employed the SVD version configured to predict 14 frames. To handle additional visible mask inputs, extra channels in the first layer were added after concatenation and initialized to zero. A freeze motion bucket and fixed frame rate were used for simplicity. During inference, conditional samples were generated using the EDM sampler with 50 steps [39], taking approximately 20 seconds to produce an output video.

B.2. Amodal Completion and Segmentation

Test Dataset In addition to the test split of OvO-Easy and OvO-Hard, we curate two additional datasets, Kubric-Static and Kubric-Dynamic, using the Kubric simulator [26] to benchmark the generalizability of the models. For Kubric-Static, we randomly select 2 to 5 objects from GSO [18], along with a background dome. The objects are placed in a static scene with randomized scales and positions. A rotating video is rendered using blender [12] by rotating the camera around the scene, capturing each object’s modal and amodal masks as well as amodal RGB images. From the rendered videos, we filter 365 samples with occlusions for benchmarking, ensuring that at least 10 out of 14 frames in each video contain occluded objects. For Kubric-Dynamic, we randomly select 2 to 3 falling objects and combine them with 2 to 4 static objects placed on the ground as well as a background dome. A linearly changing camera trajectory is applied before rendering each frame. Using the same filtering criteria as in Kubric-Static, we select 323 videos with occlusions for benchmarking.

Metrics Since a significant portion of the synthesized frames is white, this can inflate the PSNR, SSIM, and LPIPS values. To address this, we crop the synthesized amodal object using a dilated bounding box of the ground-truth (GT) amodal mask and compute the PSNR, SSIM, LPIPS, and CLIP-T metrics within this specific region.

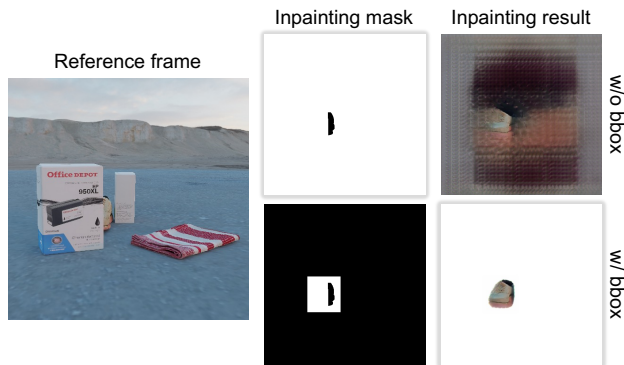


Figure S.12. **Comparison on inpainting mask.** We try two kind of inpainting mask for the E²FGVI baseline, and the one with bounding box constraint is significantly better.

Baselines Since pix2gestalt [67] can only generate images at a resolution of 256×256 , we resize all results to this resolution when calculating the metrics. For the E²FGVI baseline, we observed significantly degraded performance when masking out all but the visible object area. To address this, we first change the background to white and then use the same dilated bounding box of the ground-truth (GT) amodal mask as the inpainting mask. An illustrative comparison of the inpainting masks and the corresponding results is provided in Fig. S.12.

B.3. Object Reconstruction

Dataset We also use objects from GSO [18] to create compositional occluded scenes. Specifically, we first place a primary object at the center of the scene. Then, we select 3 to 6 additional

objects along with a background dome and arrange them around the central object to ensure occlusion occurs. Finally, we rotate the camera around the center of the scene to generate an occluded video. A total of 20 scenes are composed for benchmarking.

Reconstruction We directly apply NeRF2Mesh [80] to the synthesized results for reconstruction, where images with better cross-view consistency result in higher reconstruction quality. To enhance performance, NeRF2Mesh also requires an object mask during reconstruction. We obtain this mask by thresholding the synthesized images.

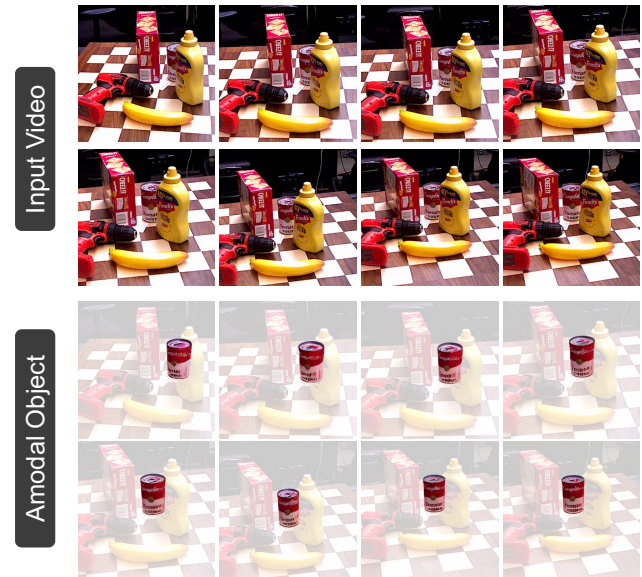


Figure S.13. **Intermediate results on YCB-Video.** We visualize the intermediate synthesized video on YCB-Video.

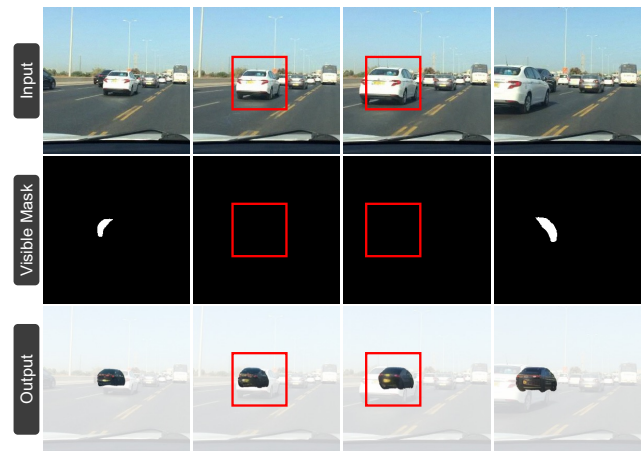


Figure S.14. **Revealing missing objects.** Our method is able to reveal missing objects by inferring from neighboring frames.

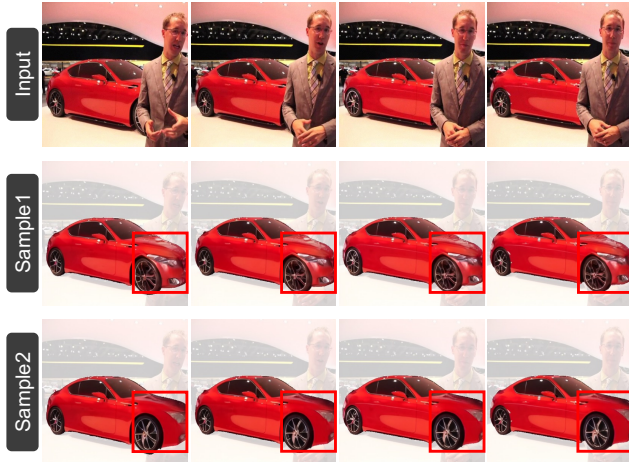


Figure S.15. **Diversity in sampling.** We can sample multiple reasonable results due to the inherent ambiguity in occluded area.

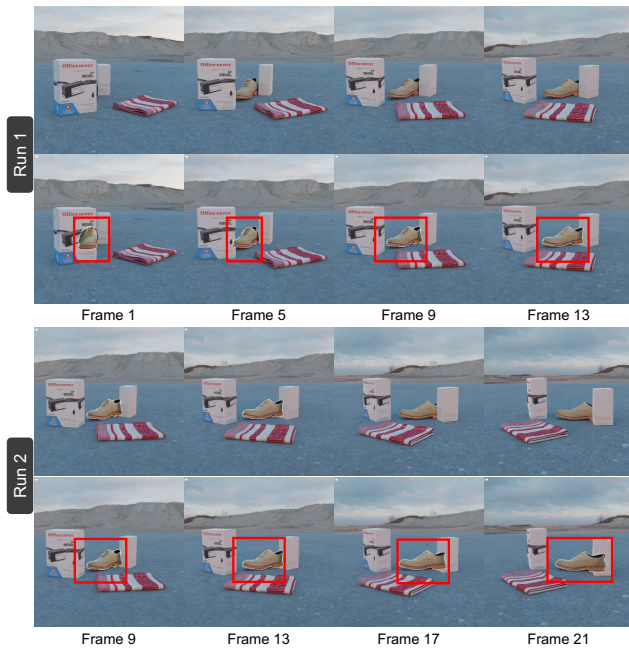


Figure S.16. **Tackling long videos.** Our method is able to extend beyond 14 frames by progressive generation.

B.4. Pose Estimation

We select a video in YCB-Video [97] and utilize SAM2 [72] to acquire the visible masks of an object throughout the video. An intermediate result (synthesized video of the amodal object) using our method is shown in Fig. S.13.

B.5. User Study

We select 20 videos from unseen datasets including ScanNet++ [14, 106], BridgeData [19, 88], YouTube-VOS [101], YCB-Video [97], and various Internet videos. Each questionnaire contains 16 questions, asking participants to evaluate the comple-

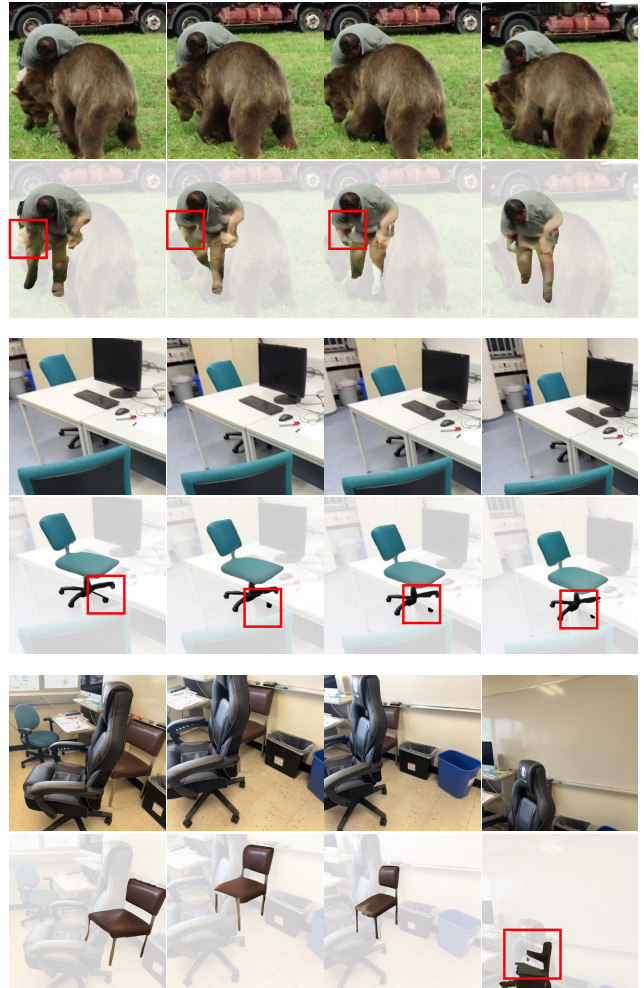


Figure S.17. **Failure cases.** Our method has limitations under certain challenging conditions. For instance, it may produce blurry results in areas with complex occlusions, as seen in the hand region of the first example. Similarly, it struggles to handle extremely fine-grained and heavily occluded structures, as demonstrated in the leg area of the second example. Additionally, our method may fail to perform effectively during drastic and sudden camera movements as shown in the last frame in the third example.

tion results across three dimensions: 1) Content-Quality: The overall quality of the completed content, 2) Content-Consistency: Temporal consistency of the completed object, and 3) Content-Plausibility: Whether the completed object is semantically aligned with its visible part. A snapshot of the questionnaire interface is shown in Fig. S.18. We gathered feedback from 36 participants, resulting in 576 valid responses.

C. Additional Results

We highly recommend browsing the anonymous local website provided in the *supplementary materials*, which contains comparisons with baselines, more qualitative results on diverse datasets, and examples of long videos. Comparison videos are also provided in the local website.

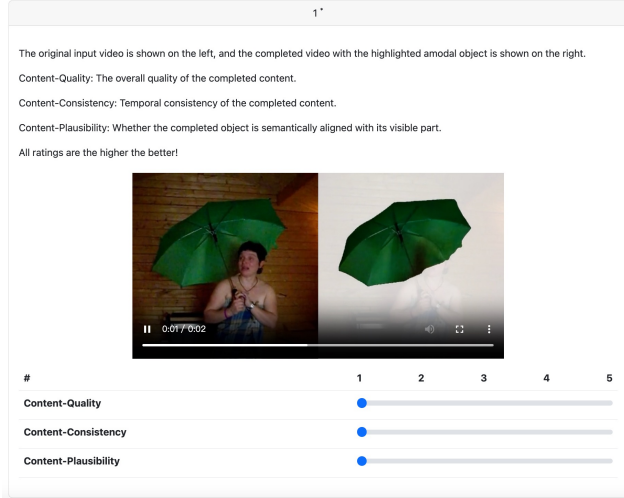


Figure S.18. Interface of the user study.

C.1. More Comparisons

We provide qualitative comparison on ScanNet [14, 106], Bridge-Data [19, 88], and YCB-Video [97] in Fig. S.19. More visualized comparisons on Bdd100k [107] and YouTube-VOS are provided in Fig. S.20. The original resolution of Bdd100k [107] used for inference is 640×384 , we crop out the region of interest for better visualization. Similarly, for pix2gestalt [67], we crop a square area as input, as the method requires square images.

C.2. More Qualitative Results

We provide more qualitative results of our method on ScanNet [14, 106] in Fig. S.21, Fig. S.22, and Fig. S.23. More qualitative results on BridgeData [19, 88] are provided in Fig. S.24, Fig. S.25, and Fig. S.26. More qualitative results on YouTube-VOS [101] are provided in Fig. S.27 and Fig. S.28. More qualitative results on YCB-Video [97] are provided in Fig. S.29 and Fig. S.30. More intuitive visualized results on various datasets and in-the-wild videos are provided in the local website attached in *supplementary materials*.

C.3. Revealing Missing Objects

An object may be completely invisible (occluded by other objects) in a video clip. We observe that our method is able to reveal completely missing objects by aggregating information from neighboring frames in certain cases. For example, as shown in Fig. S.14, the black car is completely occluded by the white car in front of it in middle frames, and our method is able to hallucinate the position, shape, and appearance of the black car.

C.4. Tackling Long Videos

To extend beyond 14 frames, we introduce a sliding window mechanism for progressively generating subsequent frames, as illustrated in Fig. S.16. In the first run, the initial 14 frames are selected, and the amodal object is synthesized. The synthesized object is then blended back into the video, as shown in the second row. For the second run, subsequent frames are concatenated with the previously blended frames as the input video. The visible

masks of overlap frames are acquired by thresholding the synthesized object. This sliding window approach allows our method to effectively generate videos exceeding 14 frames. Two additional qualitative examples are available on the local website.

C.5. Diversity in Sampling

Since amodal completion possess inherent ambiguity, we can synthesize multiple reasonable results and a qualitative example indicating the diversity is shown in Fig. S.15.

C.6. Failure Cases

We illustrate several failure cases in Fig. S.17. In the first example, nearly the entire legs and arms of the human are occluded, representing a severely occluded scenario. Under such conditions, our method may produce low-quality outputs, such as the blurry hands and occasionally missing legs. In the second example, the chair is heavily occluded by the white table. While it can be inferred that the chair has thin legs, our method may struggle with accurately reconstructing thin structures in certain frames. In the third example, the camera undergoes drastic movements, and the brown chair becomes heavily occluded from specific viewpoints. Our method struggles to recover accurate and consistent results when the object is almost missing.

D. Limitations and Negative Impacts

Limitations We have discussed about several failure cases in Appendix C.6. Additionally, our method is sensitive to resolution variations due to the constraints of the SVD architecture. While we can extend beyond 14 frames, generating extremely long videos remains a challenge. We hope that advancements in more powerful video diffusion models will help address these issues in the future. Moreover, as our method incorporates data from only a few datasets as mentioned in Appendix A.3, its performance may degrade when generalizing to vastly different domains, such as human interactions with other objects as shown in the example in Fig. S.17. Incorporating more diverse training data and curating realistic occlusion scenarios could help mitigate this issue.

Negative Impacts The use of diffusion models to generate content raises significant ethical concerns, including potential privacy violations and the risk of generating biased content. These models can be misused to spread misinformation or serve deceptive purposes, eroding trust and causing societal harm. Additionally, they may produce misleading or false outputs, causing potential challenges in fields where accuracy and reliability are crucial.

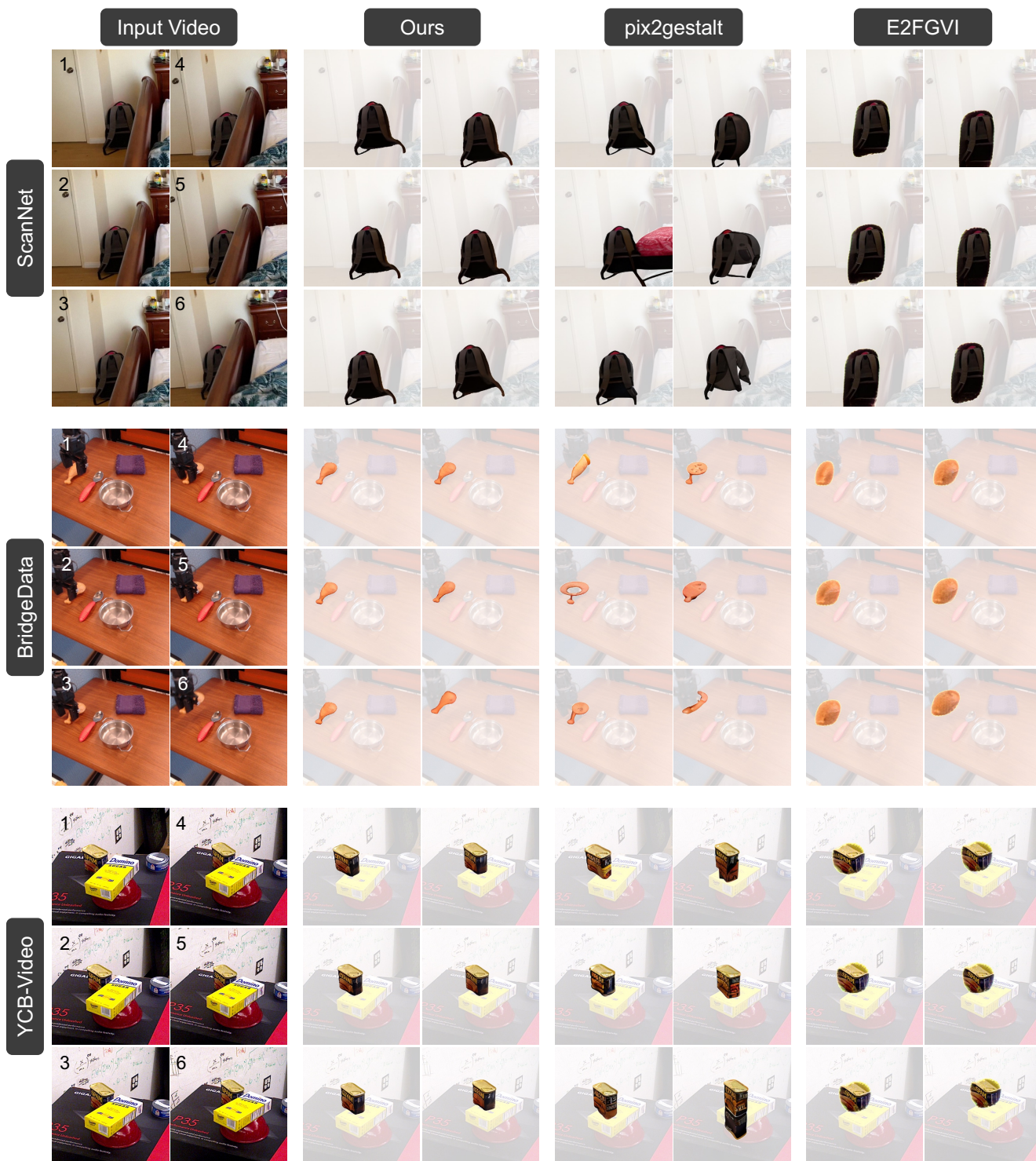


Figure S.19. Qualitative comparison on ScanNet [14, 106], BridgeData [19, 88], and YCB-Video [97].

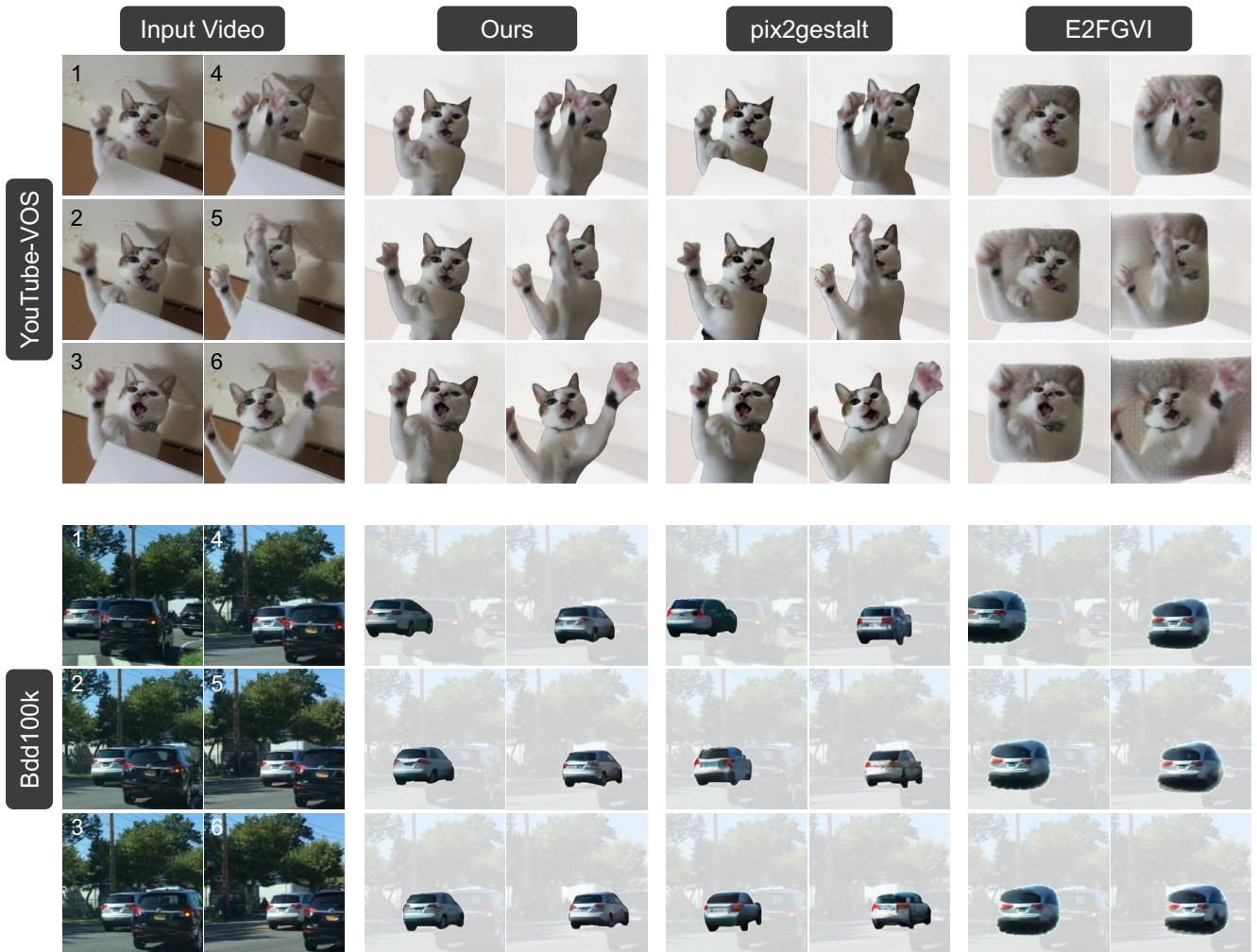


Figure S.20. Qualitative comparison on YouTube-VOS [101] and Bdd100k [107].

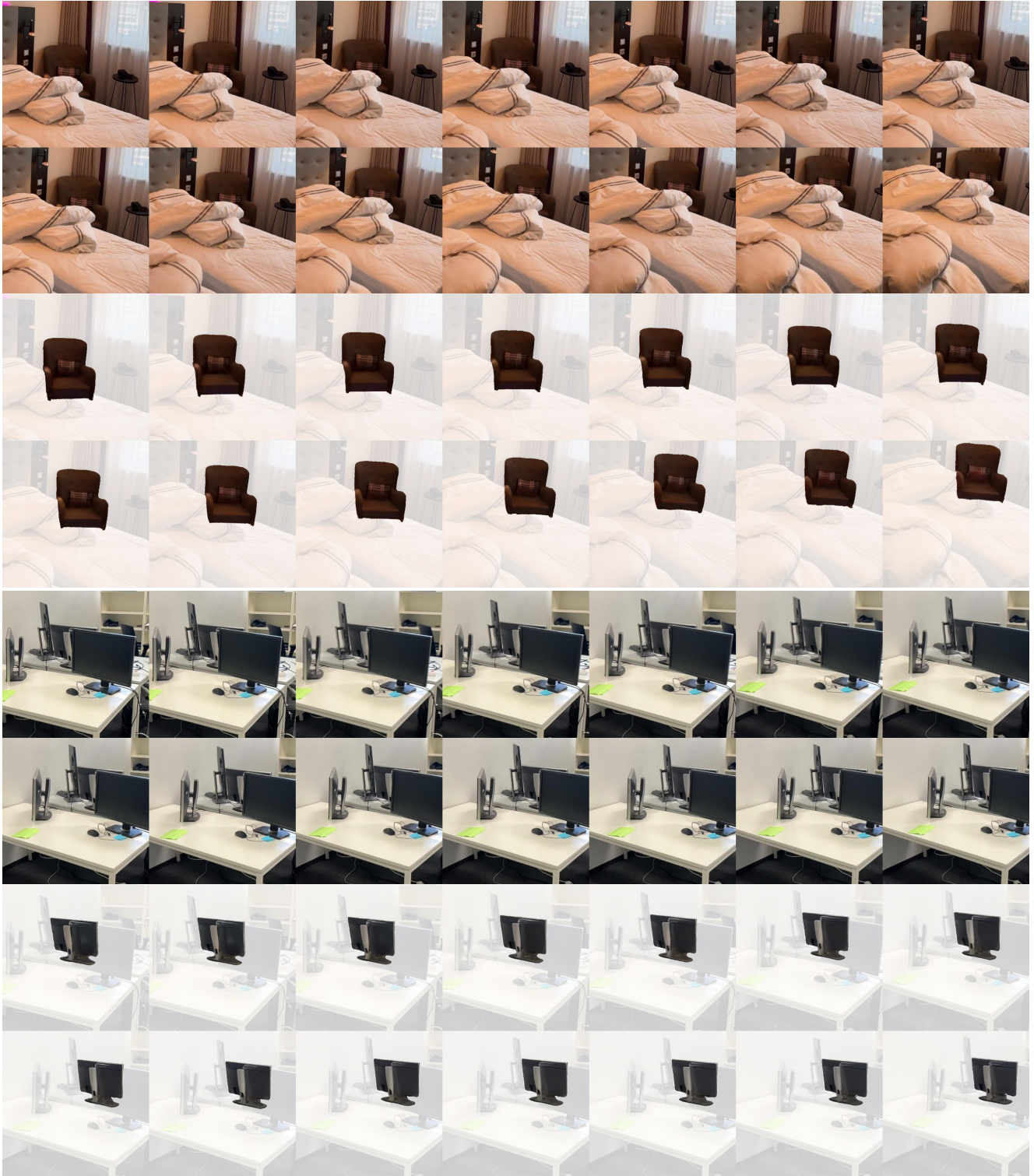


Figure S.21. Qualitative results on ScanNet [14, 106].

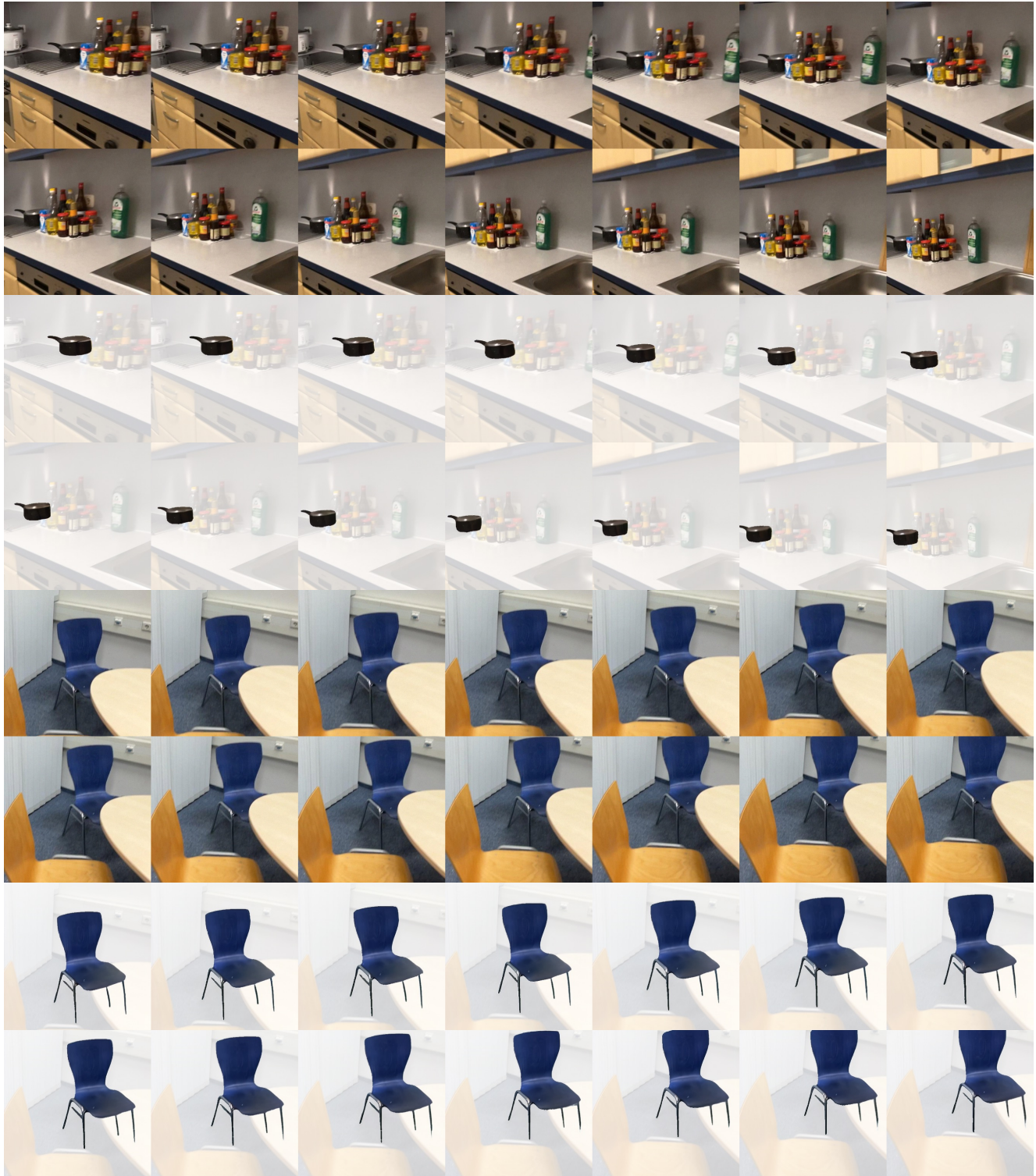


Figure S.22. Qualitative results on ScanNet [14, 106].

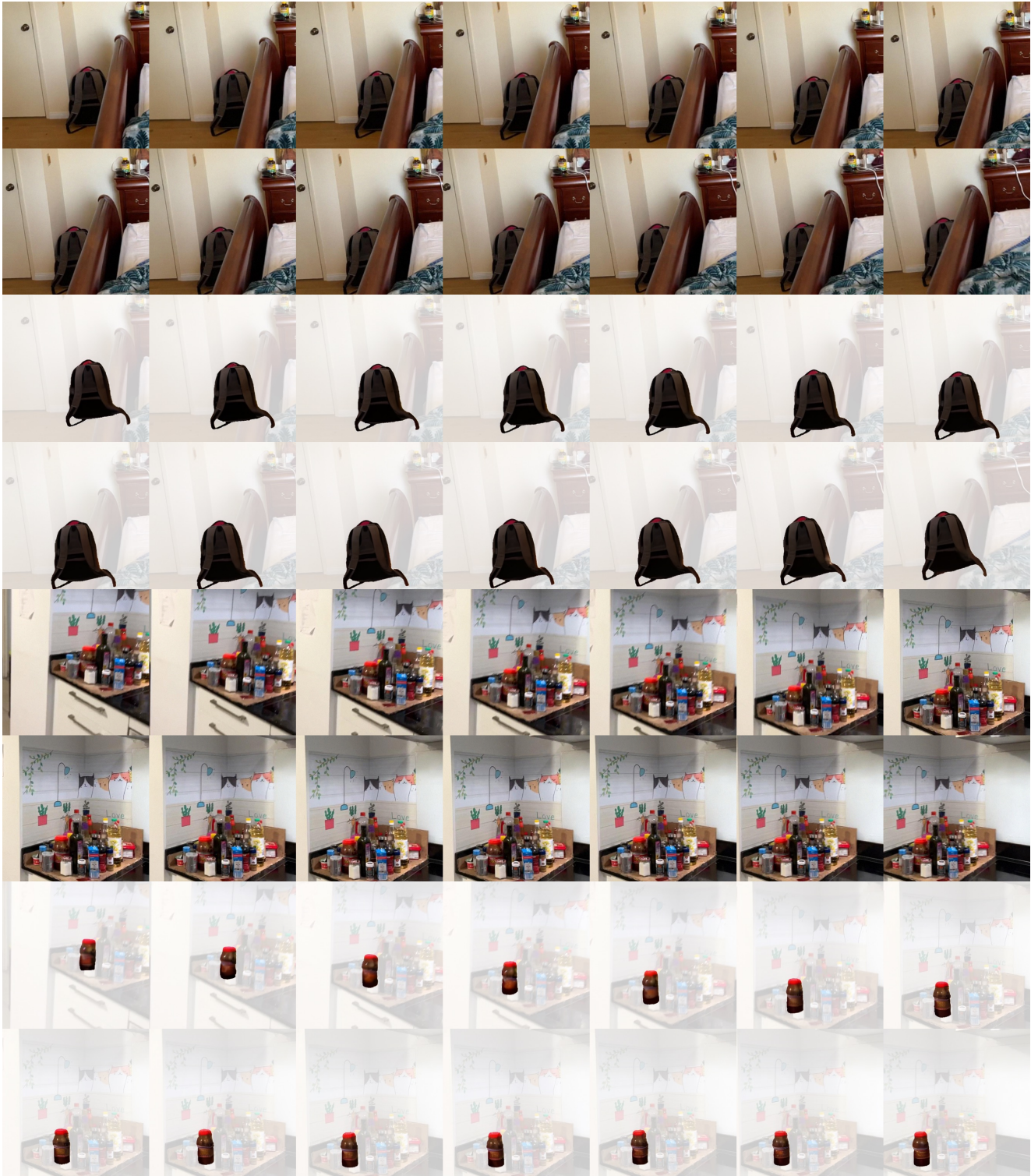


Figure S.23. Qualitative results on ScanNet [14, 106].



Figure S.24. Qualitative results on BridgeData [19, 88].

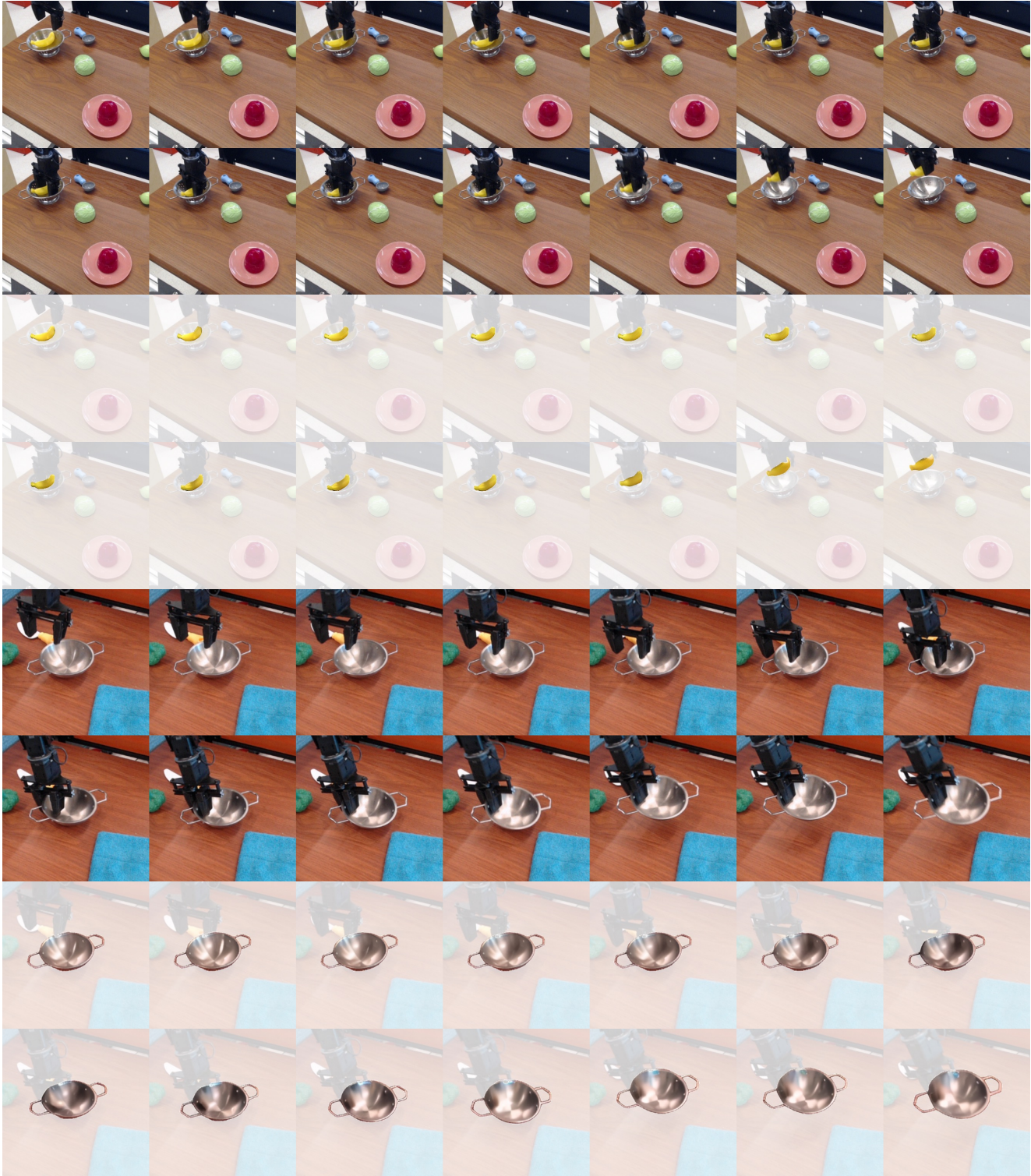


Figure S.25. Qualitative results on BridgeData [19, 88].

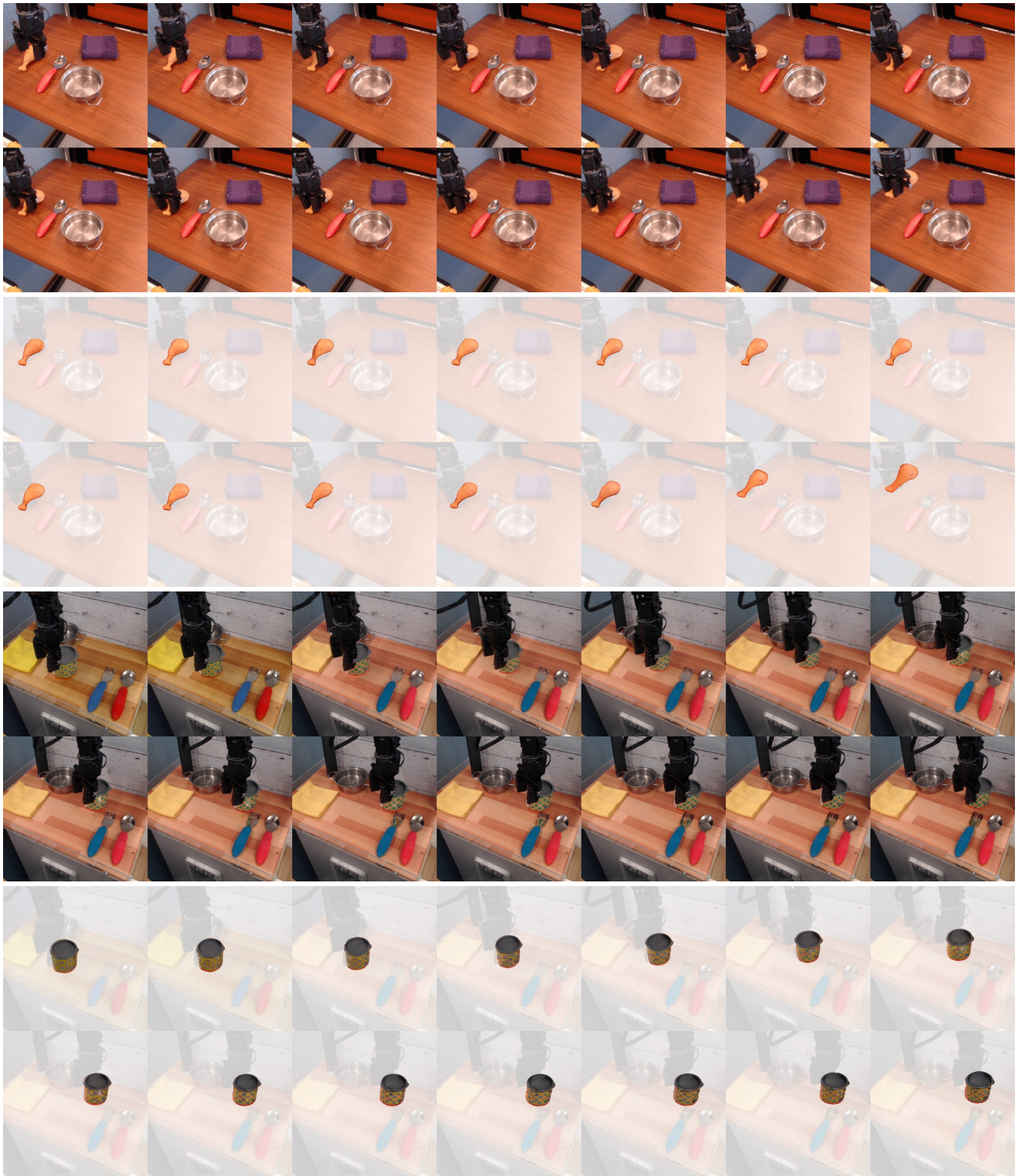


Figure S.26. Qualitative results on BridgeData [19, 88].

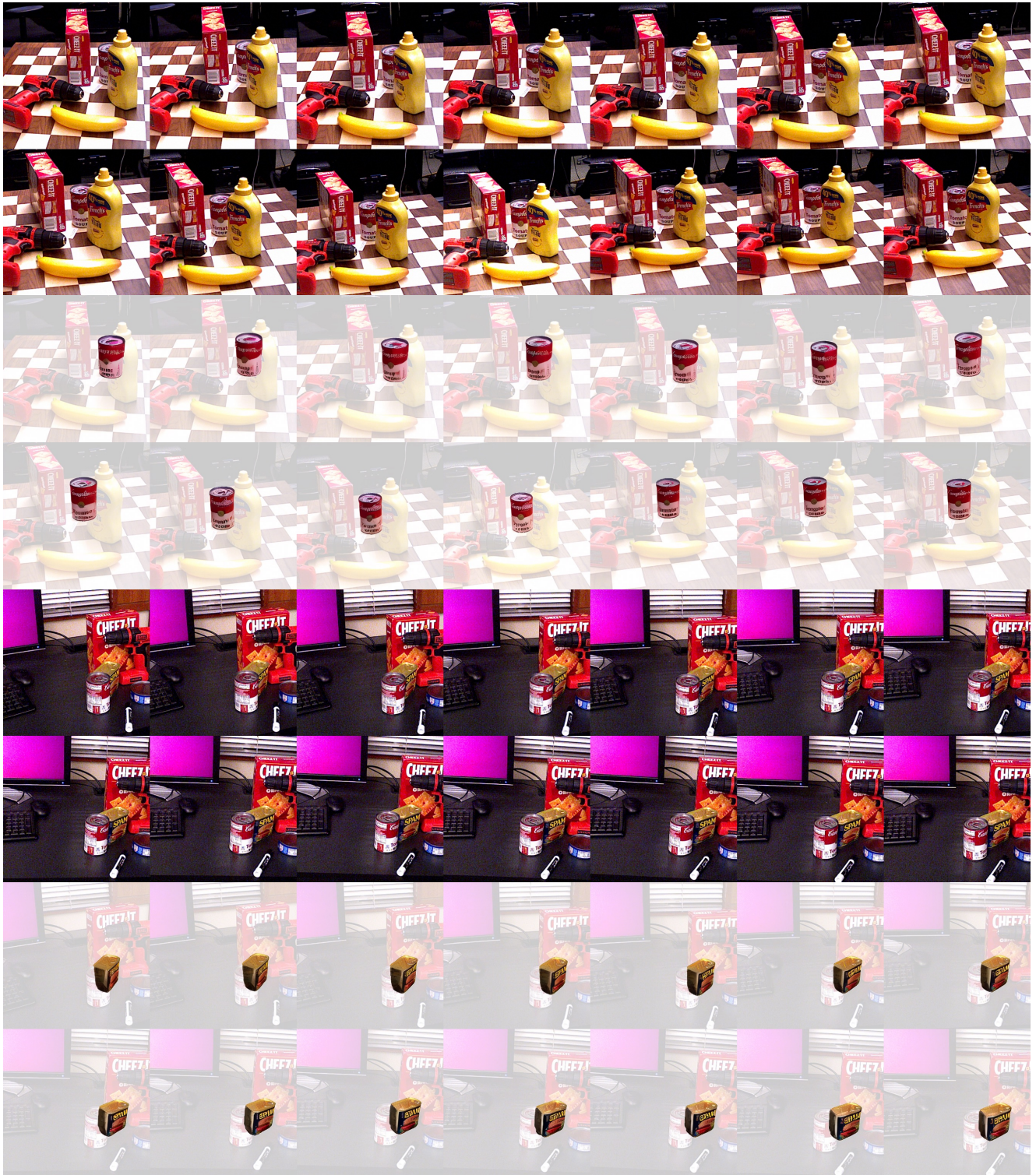


Figure S.27. Qualitative results on YCB-Video [97].



Figure S.28. Qualitative results on YCB-Video [97].

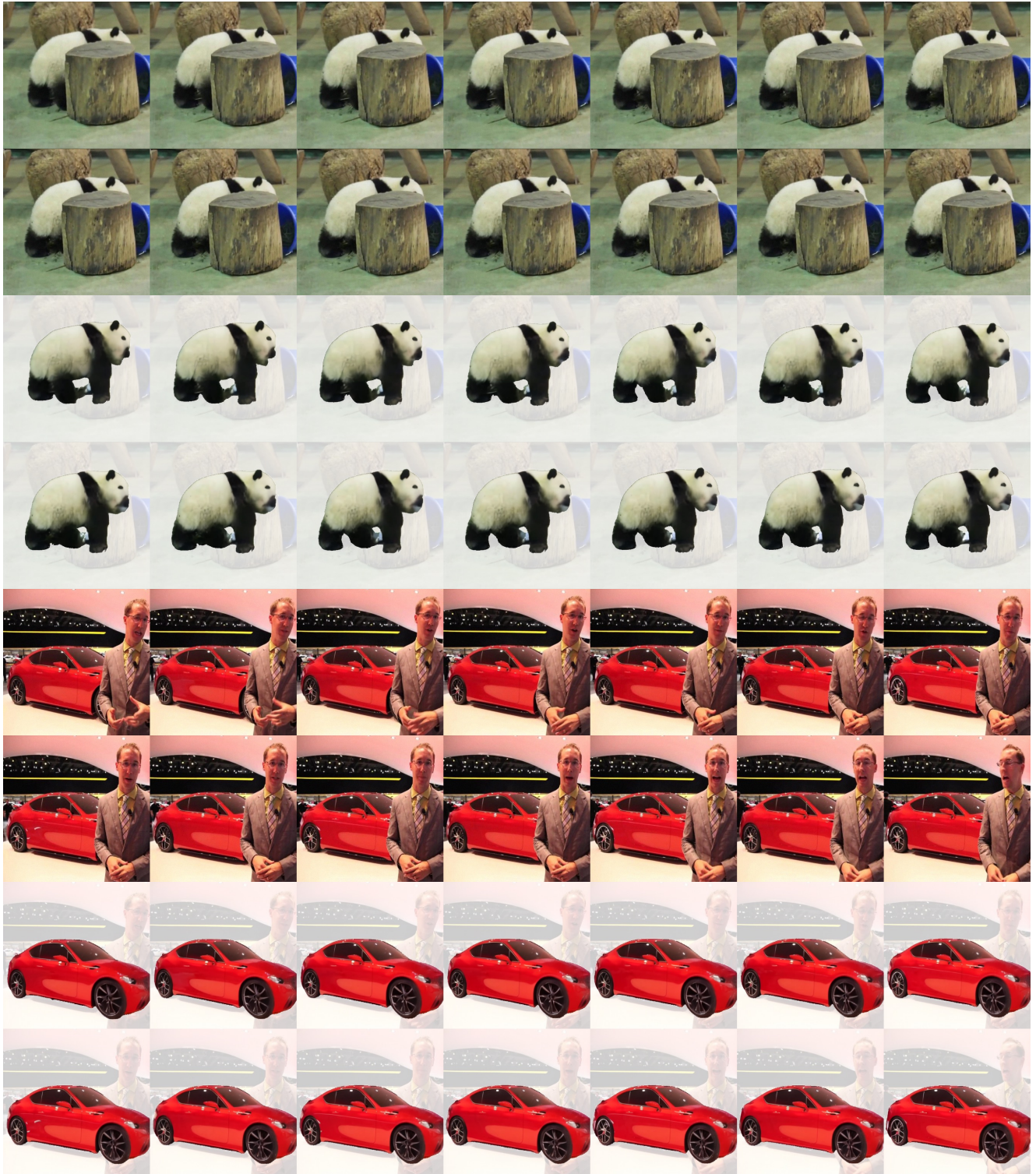


Figure S.29. Qualitative results on YouTube-VOS [101].

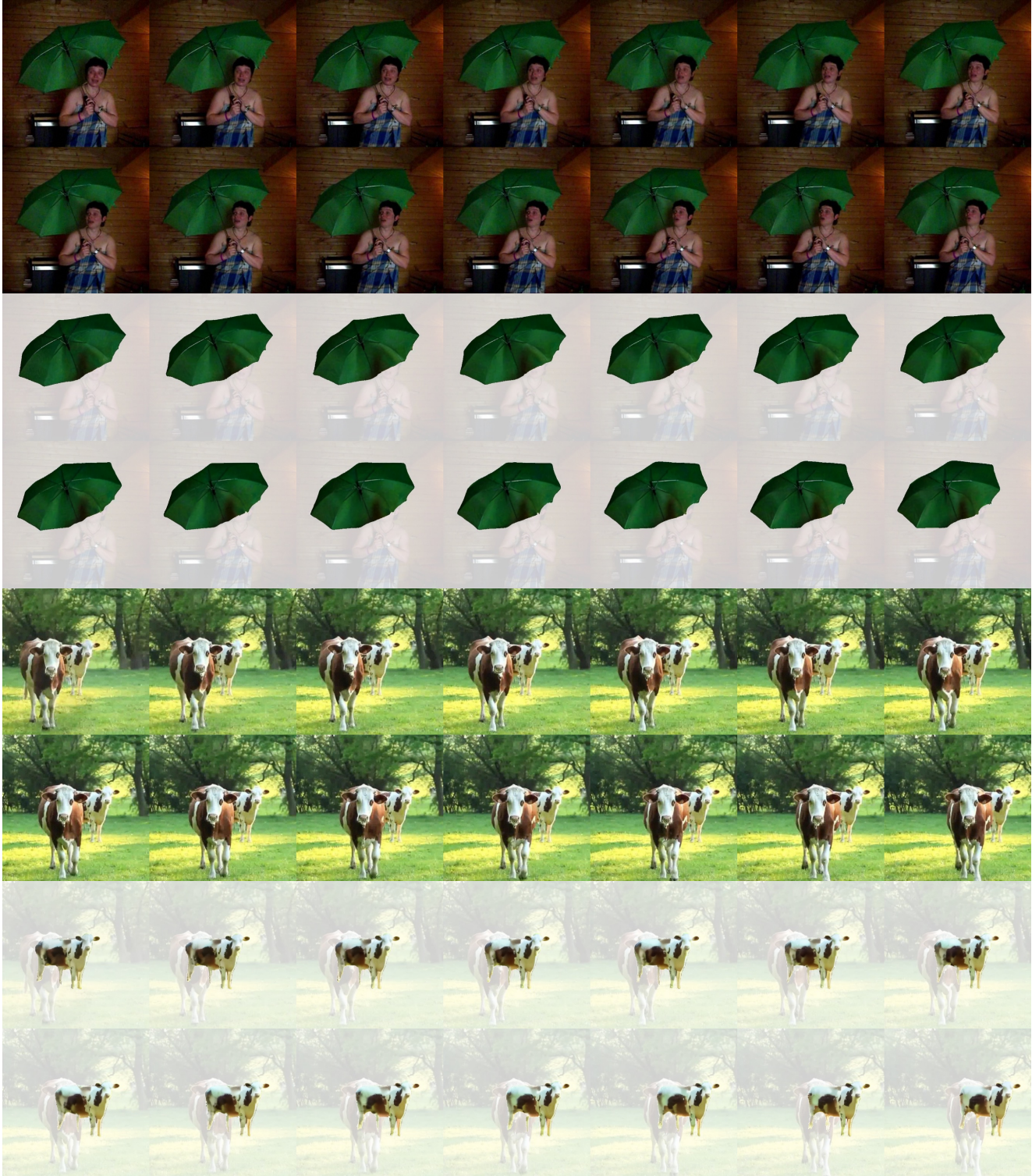


Figure S.30. Qualitative results on YouTube-VOS [101].